

Compact Symmetric Objects - II Confirmation of a Distinct Population of High-Luminosity Jetted Active Galaxies

S. KIEHLMANN,¹ A. C. S READHEAD,² S. O'NEILL,² P. N. WILKINSON,³ M. L. LISTER,⁴ I. LIODAKIS,^{5,6} S. BRUZEWSKI,⁷
V. PAVLIDOU,^{1,8} T. J. PEARSON,² E. SHELDAHL,⁷ A. SIEMIGINOWSKA,⁹ K. TASSIS,^{1,8} AND G. B. TAYLOR⁷

¹*Institute of Astrophysics, Foundation for Research and Technology-Hellas, GR-70013 Heraklion, Greece*

²*Owens Valley Radio Observatory, California Institute of Technology, Pasadena, CA 91125, USA*

³*Jodrell Bank Centre for Astrophysics, University of Manchester, Oxford Road, Manchester M13 9PL, UK*

⁴*Department of Physics and Astronomy, Purdue University, 525 Northwestern Avenue, West Lafayette, IN 47907, USA*

⁵*Finnish Center for Astronomy with ESO, University of Turku, Vesilinnantie 5, FI-20014, Finland*

⁶*Department of Physics, Univ. of Crete, GR-70013 Heraklion, Greece*

⁷*Department of Physics and Astronomy, University of New Mexico, Albuquerque, NM 87131, USA*

⁸*Department of Physics and Institute of Theoretical and Computational Physics, University of Crete, 70013 Heraklion, Greece*

⁹*Center for Astrophysics—Harvard and Smithsonian, 60 Garden St., Cambridge, MA 02138, USA*

ABSTRACT

Compact Symmetric Objects (CSOs) are compact (< 1 kpc), jetted Active Galactic Nuclei (AGN), whose jet axes are not aligned close to the line of sight, and whose observed emission is not predominantly relativistically boosted towards us. Two classes of CSOs have previously been identified: approximately one fifth are edge-dimmed and designated as CSO 1s, while the rest are edge brightened and designated as CSO 2s. This paper focuses almost exclusively on CSO 2s. Using complete samples of CSO 2s we present three independent lines of evidence, based on their relative numbers, redshift distributions, and size distributions, which show conclusively that the vast majority ($> 99\%$) of CSO 2s do not evolve into larger-scale radio sources. These CSO 2s belong to a distinct population of jetted-AGN, which should be characterized as “short-lived” compared to the classes of larger jetted-AGN, as opposed to “young”. We show that there is a sharp upper cutoff in the CSO 2 size distribution at ≈ 500 pc. The distinct differences between most CSO 2s and other jetted-AGN provides a crucial new time domain window on the formation and evolution of relativistic jets in AGN and the supermassive black holes that drive them.

Keywords: Active Galactic Nucleus, Compact Symmetric Objects, Young Radio Sources

1. INTRODUCTION

The first indication of relativistic motion in the jets of active galaxies was the asymmetric large-scale jet in M87 discovered by Curtis (1918). The next was arguably the discovery of rapid flux density variations in blazars (Dent 1965a,b), which were quickly shown by Rees (1966, 1967) to be due to relativistic motion of the emission regions towards the observer. In spite of this development, observations of the synchrotron self-absorption cutoff frequencies of radio sources with flat spectra led to the hypothesis that an “inverse Comp-

ton catastrophe” imposes an upper limit of $\sim 10^{12}$ K on the brightness temperatures of compact radio sources (Kellermann & Pauliny-Toth 1969). This appeared, at first, to be supported by Very Long Baseline Interferometry (VLBI) observations, but in these calculations the possibility of relativistic bulk motion towards the observer (Rees 1966, 1967) was not taken into account.

The first phase-coherent astronomical image ever obtained in any energy band, including the optical band, having a resolution significantly less than one arc second was produced in the first “hybrid map”, which showed an asymmetric one-sided radio jet (Wilkinson et al. 1977). Such core-jet structures were soon shown to predominate in compact radio sources (Readhead et al. 1978; Readhead 1980), making it clear that relativistic beaming determines the apparent morphology and the

observed brightness temperatures of most compact radio sources at cm wavelengths. Nevertheless, the inverse Compton catastrophe hypothesis continued to propagate, but, as shown by [Readhead \(1994\)](#), when relativistic beaming is taken into account, the brightness temperatures drop to $\sim 10^{11}$ K, and are consistent with equipartition between the magnetic field and particle energy densities in the emission regions.

It should therefore be clear that relativistic beaming greatly complicates the physical analysis of the observed radio emission of compact radio sources. In order to overcome such complications, which introduce large uncertainties in the physical properties, such as the magnetic field strength, the particle energy densities, the pressures, and the total energies of the emission regions, [Wilkinson et al. \(1994\)](#), hereafter W94, introduced the Compact Symmetric Object (CSO) classification of compact radio sources. Due to the morphological symmetry of the emission on either side of the nucleus, these objects are clearly not exhibiting strongly beamed emission towards the observer.

Unfortunately, a number of jetted-AGN have been misidentified as CSOs or CSO candidates in the literature, and many jetted-AGN whose axes are close to the line of sight, and whose observed emission is strongly beamed towards us, have crept into this class. This paper is the second of three on the morphological radio properties of CSOs in which we explore CSO phenomenology uncontaminated by objects that have been mis-identified as CSOs. In the first paper (Paper 1: [Kiehlmann et al. in press](#)) we added two new criteria, based on variability and speed, to the CSO selection criteria and undertook a detailed survey of the literature, which enabled us to identify 79 bona fide CSOs. From the 79 bona fide CSOs we determined the numbers in three complete samples¹ from which, in this paper (Paper 2), we show that $\gtrsim 99\%$ of CSO 2s form a class of jetted-AGN that is both distinct from other jetted-AGN and exhibits a sharp cutoff in size at ≈ 500 pc, and a corresponding cutoff in age at ≈ 5000 yr, so that only fewer than 1% of CSO 2s might possibly go on to form the larger classes of jetted-AGN, such as Fanaroff and Riley Type I (FRI) and Type II (FR II) objects ([Fanaroff & Riley 1974](#)). In the third paper (Paper 3: [Readhead et al. in press](#)) we discuss the evolution of CSO 2s and show that while they are nearly all “short-lived” compared to the classes of larger jetted-AGN, only a minority of them are “young”. Note that FR I and FR II objects have

sizes in the ~ 20 kpc – several Mpc range, and therefore clearly have ages much longer than the vast majority of CSO 2s. We should avoid the implicit assumptions involved in calling all CSO 2s “young”, which obscure the true nature and importance of this class of jetted-AGN. It is critically important, therefore, to recognize the distinction between the terms “young” and “short-lived”, which otherwise obfuscate the phenomenology of the CSO class.

In an important development in the study of CSOs, [Tremblay et al. \(2016\)](#) showed that there are two major morphological classes of CSOs: edge-dimmed objects, which we designate as CSO 1s, and edge-brightened objects, which we designated as CSO 2s. Paper 1 confirms their finding and this paper deals almost exclusively with CSO 2s.

As discussed in detail in Paper 1, in CSOs, two emission regions are seen straddling the center of activity, making it clear that these cannot be strongly relativistically boosted, otherwise the object would be seen as a one-sided asymmetric “core-jet” object as is the case in the vast majority of compact radio sources observed at cm wavelengths ([Kellermann et al. 1998](#); [Lister et al. 2019](#)).

Individual CSO 2s undergo appreciable evolutionary structural changes on timescales of years that can therefore be studied without the complications of relativistic beaming. The bulk flows along their jets and their speeds of advance into the interstellar medium can be measured directly. We argue that CSO 2s provide a uniquely accessible time domain laboratory for the study of relativistic jets ([Blandford et al. 2019](#)) and the SMBH central engines that drive them, because they are short-lived compared to the classes of larger jetted-AGN, rather than young, and hence pass through all stages of their lives as CSO 2s, which are therefore available for detailed study in all phases of their lives. It is important to distinguish between CSOs that have small sizes because they are “short-lived” compared to larger classes of jetted-AGN, and CSOs that have been stalled by the interstellar medium of their host galaxies and therefore stopped growing in size. We propose the hypothesis that such stalled CSOs are likely to be edge-dimmed and hence fall into the CSO 1 class. We also note in passing that this could be of great importance to feedback. As we show in Paper 3, the most luminous CSO 2s that are the subject of this study have not been stalled – their hot spots are separating on average at $\sim 0.4c$, and their maximum lifetimes are ~ 5000 yr. For the purposes of this study, although stalled CSO 2s are of great potential interest, we do not consider them further in these three papers. A minority of the less lu-

¹ A “complete sample” is defined to be a sample that includes all objects down to a given flux density limit over a given area of sky ([Pooley & Ryle 1968](#); [Schmidt 1968](#); [Longair & Scheuer 1970](#))

minous CSO 2s in our study might possibly be stalled systems and should also be considered in that light. But this is beyond the scope of the present study.

By the early 1990s, three bona fide CSO 2s had been definitively identified in the complete sample of 65 radio sources studied by [Pearson & Readhead \(1988\)](#). Despite the small size of the CSO sample, and entirely because it was part of a complete sample, this sample of only three CSO 2s was enough to enable a number of the most critical questions about CSO 2s to be addressed by [Readhead et al. \(1994\)](#), hereafter R94, including their relationship to the larger jetted-AGN, their lifetimes, and their energy requirements. R94 concluded that CSO 2s form a distinct population of compact jetted-AGN, and that there must be a physical reason for this which provides a unique window on the central engines that drive AGN. R94 also suggested that CSO 2s might be the result of the capture of a single star by a SMBH in an otherwise quiescent elliptical galaxy nucleus. This possibility was also suggested more recently by [An & Baan \(2012\)](#).

All of these properties of CSO 2s were discussed in more detail, and confirmed, in [Readhead et al. \(1996\)](#), hereafter R96. Nevertheless, in spite of their distinction, CSO 2s have attracted comparatively little attention among jetted-AGN enthusiasts. We explore the characteristics of CSO 2s in considerably more detail in this paper and in Paper 3.

The CSOs are a subset of AGN, but by studying a restricted well-defined sample of CSOs we aim to understand them in depth and gain new insights into the physics and formation of jetted-AGN. Although it is not a primary goal of these papers, we discuss the relationship of CSOs to other classes of AGN where appropriate in this paper and in Paper 3. To place CSOs in the broader context of compact radio sources associated with AGN, the reader is referred to the comprehensive review of [O’Dea & Saikia \(2021a\)](#), hereafter OS21.

Throughout this paper we adopt the convention $S_\nu \propto \nu^\alpha$ for spectral index α , and use the cosmological parameters $\Omega_m = 0.27$, $\Omega_\Lambda = 0.73$ and $H_0 = 71 \text{ km s}^{-1} \text{ Mpc}^{-1}$ ([Komatsu et al. 2009](#)). We do this for consistency with our other papers. None of the conclusions would be changed were we to adopt the best model of the Planck Collaboration ([Planck Collaboration et al. 2020](#)).

2. COMPLETE SAMPLES OF JETTED-AGN

The disposition of the CSOs we consider in this study, amongst the CSO 1 and CSO 2 classes, the CSOs with spectroscopic redshifts and those without, and the CSOs

Table 1. The CSO Samples

	CSO 1	CSO 2	All
With spectroscopic redshift	11	43 (17)	54
Without spectroscopic redshift	5	20 (2)	25
All	16	63 (19)	79

NOTE—This Table shows the numbers of bona fide CSOs of classes 1 and 2 identified in Paper 3, with and without spectroscopic redshifts. Numbers in parentheses indicate bona fide CSOs in the PR+CJ1+PW complete samples. In this paper we deal almost exclusively with the 17 CSOs in these complete samples that have spectroscopic redshifts.

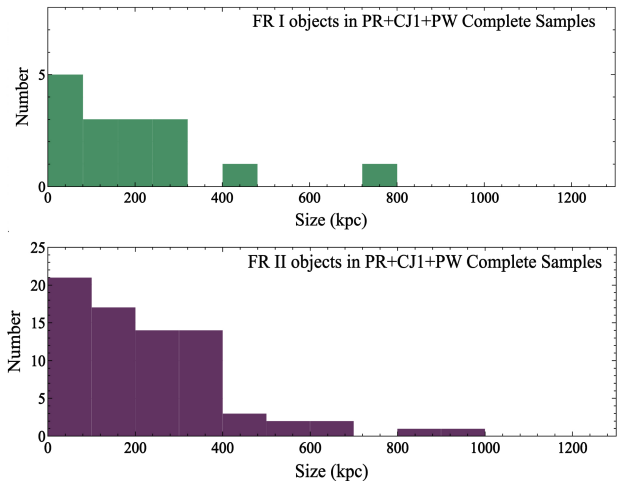


Figure 1. The distributions of the largest projected sizes of FR I objects (top panel) and FR II objects (bottom panel) in the PR+CJ1+PW complete samples. The FR I sizes have been determined from our own angular size measurements. The FR II sizes are based on the largest angular size measurements of [Nilsson et al. \(1993\)](#) for all but six sources not included in their sample, for which we measured the angular sizes ourselves. There is one FR II object (3C 236) of size 4.3 Mpc that is not included in the FR II plot.

in complete samples is shown in Table 1. The classification of CSO 1s and CSO 2s that we use here is discussed in more detail in Paper 3.

We use only complete samples for statistical tests in this paper. Other methods for making statistical tests, which are not based on complete samples, must introduce some assumptions regarding the population under study, and we wish to avoid making such assumptions. We use three complete samples extensively (see Table 2): (1) The 5 GHz Pearson–Readhead (PR) complete sample ([Pearson & Readhead 1988](#)) based on the

MPIFR/NRAO S4 and S5 surveys (Pauliny-Toth et al. 1978; Kuehr et al. 1981); (2) The first Caltech–Jodrell (CJ1) 5 GHz complete sample (Polatidis et al. 1995; Xu et al. 1995); (3) The Peacock–Wall (PW) 2.7 GHz complete sample (Peacock & Wall 1981; Wall & Peacock 1985).²

There are 282 objects in the union of these three complete samples and these are listed in Table 7 in the Appendix. In our analysis in this paper, we exclude M82 (3C 231) which is in the PR and PW samples, but is a starburst galaxy and not a jetted AGN, leaving 281 sources. In Paper 1 we listed the number of CSOs in the three complete samples. The number of CSO 2s in each of these three complete samples is given in Table 2. The determination of a uniform set of measurements of the largest angular size of the 79 bona fide CSOs is described in Paper 1.

All the sources in the PW sample were mapped using the Cambridge 5 km Telescope by Peacock & Wall (1981), who also classified the large scale structures in the PW sample according to the following types: (i) FR I and FR II, and an intermediate FR type (FR?); (ii) objects unresolved on the 5 km Telescope (U); (iii) Compact Steep Spectrum (CSS) objects having $\alpha \leq -0.5$ between 2.7 GHz and 5 GHz; and (iv) double objects with the optical identification coincident with one of the two radio components. These types are listed in column 7 of Table 7 in the Appendix.

Discussions of a size cutoff in CSO 2s are not new (Augusto et al. 1998, 2006; Augusto 2009), and early lobespeed measurements showed that the hotspots of CSO 2s are rapidly separating (Owsianik & Conway 1998; Owsianik et al. 1999; Polatidis et al. 2002). It was clear, therefore, as pointed out in R94 and R96, that CSO 2s must be short-lived, since otherwise there would be far more of their longer-lived, larger counterparts. This means that CSO 2s *must* exhibit a size cutoff. As shown in this paper, we have now determined that a sharp cutoff occurs at ≈ 500 pc. The evolution of the vast majority of CSO 2s from “early-life” through “mid-life” to “late-life” is discussed in detail in Paper 3, where we also discuss the fact that a small fraction ($< 1\%$) of CSO 2s almost certainly go on to form the larger classes of jetted-AGN, including MSOs, FR Is and FR IIs.

Since the CSOs in the PR+CJ1+PW complete samples are all CSO 2s, the findings of this paper apply, (i) only to CSO 2s, and (ii) only to the high-luminosity end of the CSO 2 luminosity function. Much deeper

complete sample surveys, in which we are engaged, are needed to expand our knowledge into the low-luminosity regime of CSO 2s. It should therefore be born in mind that our sample, comprising only 17 objects, is small, so that a degree of caution must be exercised in interpreting the results. For this reason we present all of the relevant statistics and p-values so that readers may judge for themselves the significance of the results.

There are precedents in astronomy for drawing powerful conclusions based on small numbers. For example, Hubble (1929a,b), based his discovery of the expansion of the universe on measurements of just 22 galaxies. Minkowski (1941) had just 14 supernovae for his classification of Type I and Type II supernovae, with 9 and 5 objects, respectively. Closer to the approach of this paper, there is also a powerful precedent for using well-defined statistical tests based on complete samples in the paper by Schmidt (1968), who used a complete sample of just 33 quasars to demonstrate convincingly that quasars are not evenly distributed in space, but show strong cosmological evolution.

In this paper we present three independent sets of data and lines of argument based on complete samples, each of which shows that the vast majority of CSO 2s form a distinct population of jetted-AGN. These lines of argument are based on (i) the numbers of CSO 2s in complete samples; (ii) the redshift distributions of these CSO 2s; and (iii) the size distribution of these CSO 2s. Of these, the results of first and third arguments are, in our view, compelling. The results of the second argument (ii) are significant only at the p -value= 1.6×10^{-2} (2.1σ) level, and are, therefore, not compelling, but they are in the same sense as the other two arguments – i.e. they strongly suggest that the CSO 2s are drawn, predominantly, from a distinct population of jetted-AGN.

The PW sample was selected at 2.7 GHz, unlike the PR and CJ1 samples which were selected at 5 GHz. However, we have 5 GHz flux densities for all the PW sources (Pauliny-Toth 1977). Following a suggestion by John Peacock, in order to be able to combine results from these three complete samples without introducing any possible biases due to the different sample selection frequencies, we define a subset of the PW sample that is effectively complete at 5 GHz. For this purpose we compare the GB6 (Gregory et al. 1996), PR, and PW samples at 5 GHz over their common sky area ($35^\circ \leq \delta \leq 75^\circ$, $|b| \geq 10^\circ$, B1950). These surveys were all made on different instruments at different times

² The original PW sample Peacock & Wall (1981) contained 168 sources; to these three (DA 240, 0945+73 = 4C 73.08, and NGC 6251) were added by Wall & Peacock (1985).

Table 2. The Numbers of CSS, FR I, FR II, and CSO objects in the Complete Samples.

Complete Sample	Flux Density limits	CSS Number	FR I Number	FR II Number	Total Number	CSO2 Number	CSO2/FR II Percentage	CSO2/Total Percentage
PR	$S_5 \geq 1.3$ Jy	6	3	16	64 [†]	6	37.5±18.0 %	9.4±4.0 %
CJ1	$1.3 \text{ Jy} \geq S_5 \geq 0.7$ Jy	23	6	30	135	6 [‡]	20.0±8.9 %	4.4±1.9 %
PR+CJ1	$S_5 \geq 0.7$ Jy	29	8	46	199 [†]	12 [‡]	26.1±8.5 %	6.0±1.8 %
PW	$S_{2.7} \geq 1.5$ Jy	26	15	65	170 [†]	13 [*]	20.0±6.1 %	7.6±2.2 %
PWS	$S_5 \geq 1.3$ Jy	7	8	11	50	5	45.5±24.5 %	10.0±4.7 %
PR+CJ1+PW	-	43	16	76	281 [†]	19 ^{‡*}	25.0±6.4 %	6.8±1.6 %

NOTE—All of the CSOs in the PR+CJ1+PW sample are CSO 2s. In addition, all of the PW CSOs at $\delta \geq 35^\circ$ are in the PD+CJ1 sample. [†] the numbers exclude 3C 231 (M82), a starburst galaxy, not an AGN. [‡] the numbers include the bona fide CSO J1335+5844, for which there is no published spectroscopic redshift. ^{*} the numbers include the bona fide CSO J1416+3444, for which there is no published spectroscopic redshift. These numbers are taken from the list of the 282 sources in the three complete samples given in Table 7 in the Appendix. PWS is the subsample of PW at $10^\circ < \delta < 35^\circ$ (B1950) and with $S_{5 \text{ GHz}} > 1.3$ Jy. As should be clear in view of the size of the samples, and assuming there is no dependence of the CSO fraction on flux density, the most reliable statistic is the final one combining the three full samples PR, CJ1, and PW.

Table 3. Redshifts and Sizes of the 17 CSO 2s with spectroscopic redshifts in the PR, CJ1 and PW Complete Samples

IAU Name	Redshift	Size (pc)	PR	CJ1	PW
J0029+3456	0.517	180			Y
J0111+3906	0.668	56	Y		
J0119+3210	0.0602	115			Y
J0405+3803	0.05505	44		Y	
J0713+4349	0.518	217	Y		Y
J1035+5628	0.46	221	Y		Y
J1227+3635	1.975	499		Y	Y
J1244+4048	0.8135	529		Y	
J1326+3154	0.37	345			Y
J1347+1217	0.121	215			Y
J1400+6210	0.431	378	Y		Y
J1407+2827	0.077	16			Y
J1609+2641	0.473	362			Y
J1735+5049	0.835	61		Y	
J1944+5448	0.263	196		Y	
J2022+6136	0.227	104	Y		Y
J2355+4950	0.237	337	Y		Y

NOTE—References for the redshifts and sizes are given in Paper 1.

and since many of the sources are variable the samples change slightly with time. In this area of sky, the GB6 survey has 54, the PR survey has 51, and the PW survey has 54 objects with $S_{5\text{ GHz}} \geq 1.3\text{ Jy}$. It may safely be assumed, therefore, that the PW sample is effectively complete down to 1.3 Jy at 5 GHz. Of these we define a sub-sample, PWS, where “S” stands for “Subsample”, consisting of the PW sources at declinations $\delta < 35^\circ$ (B1950) and having $S_{5\text{ GHz}} \geq 1.3\text{ Jy}$, for use in our physical size distribution statistical tests in §5. We point out that all of the PW CSOs at $\delta \geq 35^\circ$ are in the PW+CJ1 sample.

The great strength of the PR, CJ1, and PW samples is that *all* of the objects are well-studied and their radio properties on both large and small scales are known. There is, therefore, no danger of unknown selection bias that could compromise the statistics. In Table 7 in the Appendix we list all of the sources in the complete PR, CJ1 and PW samples and we provide references to these structure observations. Clearly, the references given in Table 7 do not include all of the papers that refer to the objects in these samples – in many cases we provide only a single reference to a paper that contains a good map of the object.

In addition to the above three complete samples, there is one other complete sample that is of prime importance to this study: the GaLactic and Extragalactic All-Sky Murchison Widefield Array (GLEAM) survey (Callingham et al. 2017), which covers the sky area $\delta < 30^\circ$ (J2000), $|b| > 10^\circ$ and defines a complete sample of 11,400 objects exhibiting flux densities greater than 1 Jy in the 72 MHz – 700 MHz range.

In the following sections, using the complete samples, we provide three lines of argument that the vast majority of CSO 2s form a distinct population of jetted-AGN.

3. THE FRACTIONS OF CSO 2s IN COMPLETE SAMPLES

It is important to note that, in addition to the identification of 79 “bona fide” CSOs in Paper 1, we also identified 167 “class A” CSO candidates, which are objects showing clear double structure, but for which the maps are not of sufficient quality to confirm them as CSO 2s. We have VLBA observations of these and are in process of analyzing them. We also identified 1164 “class B” CSO candidates, most of which are far less likely to be CSO 2s, but which cannot yet definitively be ruled out.

R96 gave a detailed discussion of the CSO fractions in the PR and CJ1 complete samples. Here we update this discussion and also incorporate the PW sample.

While the PR CSO sample is complete, as can be seen in Paper 1, in CJ1 there are 5 class A CSO candidates which might possibly be bona fide CSO 2s. All of these candidates have sizes less than 500 pc, and, were we to include these five sources in our analysis, the conclusions below would be strengthened. We prefer to take the conservative route and not to include any CSO candidates in the bona fide sample until they have met the CSO criteria laid out in Paper 1.

As can be seen in Paper 1, there are also six class B CSO candidates in the PR, CJ1, and PW samples. These are much less likely to be bona fide CSO 2s, and all but one have sizes less than 500 pc. For these reasons, the conservative approach is again not to include any of these objects in the present analysis.

We see in Table 2 that the fraction of CSO 2s in complete 2.7–5 GHz samples is $(6.8 \pm 1.6)\%$. This would rise to $(8.5 \pm 1.8)\%$ if all of the class A CSO 2s candidates in the CJ1 sample are shown to be bona fide CSOs.

We take as a simple hypothesis to be used throughout this paper, that, between their appearance and disappearance, the separation speed, v_{sep} , of the opposing hot spots in CSO 2s, when averaged over a sufficient interval of time, is constant, and that they continue at the same separation speed if they expand to form larger classes of sources, such as FR IIs. Under this hypothesis, the number of objects in different size ranges scales simply in proportion to the size ranges.

It is important to note that, for the purposes of our arguments regarding the fractions of CSO 2s with respect to classes of larger sources, this hypothesis is highly conservative. We show in Paper 3 that the separation speed of the hot spots for CSO 2s is $v_{\text{sep}} = (0.36 \pm 0.04)c$, whereas, for example, Carilli et al. (1991) argue convincingly that for the opposing hot spots in Cygnus A, $0.01c < v_{\text{sep}} < 0.05c$. Note that this deduced separation speed for Cygnus A is typical for FR IIs (Scheuer 1995). Based on these values, the separation speeds in CSO 2s are approximately an order of magnitude greater than those in FR IIs, which means that if CSO 2s do expand to form FR IIs, they spend far less of their time in the 0 kpc to 1 kpc size range than under the constant speed hypothesis, and so there should be even fewer of them relative to FR IIs than under the constant speed hypothesis.

Under the constant speed hypothesis we also assume that the luminosity does not change enough for the source to drop out of the flux-limited sample. We discuss possible changes in luminosity later.

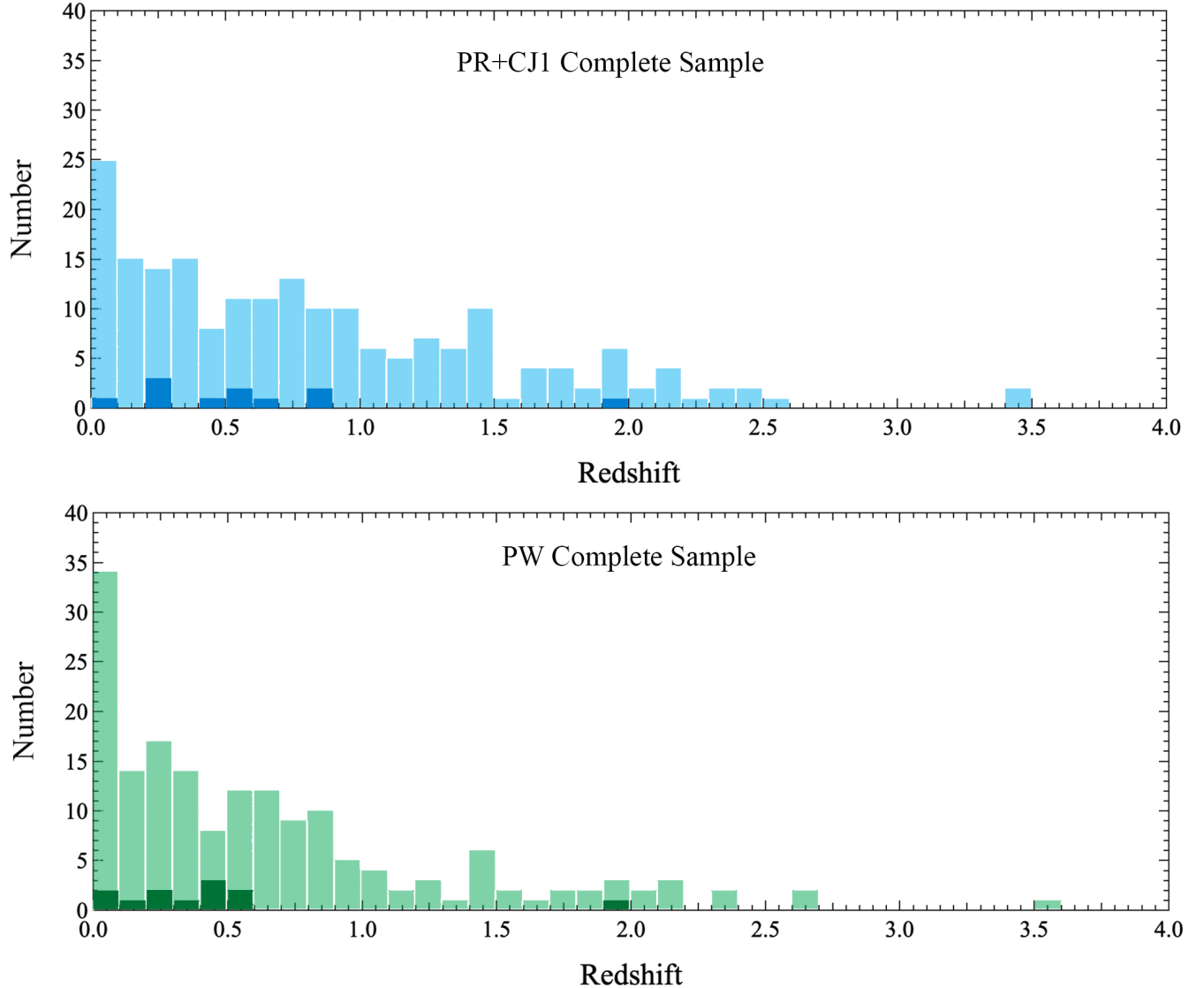


Figure 2. The redshift distributions for the PR+CJ1 complete sample (top panel) and the PW complete sample (bottom panel). The light shaded distributions show the complete samples. The dark shaded regions show the CSO 2s. Note that these distributions are not stacked vertically, so the values on the ordinate represent the total numbers of sources and the numbers of CSO 2s in each sample. The cumulative distributions and KS statistics are shown in Figs. 3 (a) and (b).

We consider three populations of objects that are larger than CSO 2s and that might, therefore, be the populations that CSO 2s evolve into:

(i) CSS objects (Peacock & Wall 1982), including the subclass of Medium Symmetric Objects (MSOs) which have sizes in the range 1 kpc – 20 kpc (Fanti et al. 1995) and R96. Note that MSOs have the same characteristics as CSO 2s apart from the size range.

(ii) Fanaroff & Riley Class I jetted-AGN (Fanaroff & Riley 1974), which have sizes that range up to ≈ 1 Mpc – see Fig. 1(upper panel).

(iii) Fanaroff & Riley Class II jetted-AGN (Fanaroff & Riley 1974), which also have sizes that range up to ≈ 1 Mpc – see Fig. 1(lower panel).

Note that Fanti et al. (1995) and R96 used an upper size limit of $15h^{-1}$ kpc for MSOs, where $H_0 = 100h$ km s $^{-1}$ Mpc $^{-1}$. For our adopted cosmology, this translates to 21 kpc. However, since the original choice of $15h^{-1}$ kpc was chosen by Fanti et al. (1995) and R96 to be a convenient “round number”, we will follow that practice and use 20 kpc as the upper size limit of MSOs in this study, which also accords with the upper limit on MSO and CSS sizes adopted by OS21.

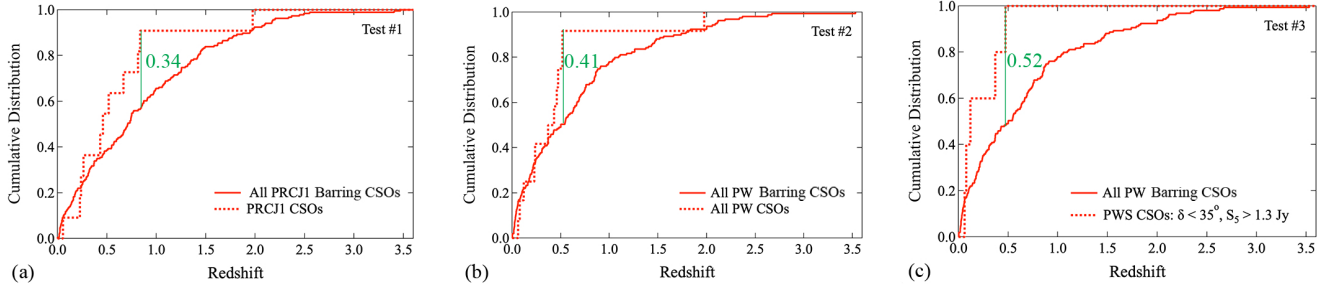


Figure 3. KS Tests on the redshift distributions of the bona fide CSO 2s in the PR+CJ1, PW, and PWS samples. (a), (b) and (c): comparison of the CSO cumulative redshift distributions *vs.* the non-CSO 2s in the complete PR+CJ1, PW, and PWS samples, respectively. The green bars indicate the maximum differences in the cumulative distributions, corresponding to the values of the KS statistic given by the numbers in green. The corresponding p-values are listed in Table 4.

Table 4. Two-sample KS Tests of CSO Redshifts as a Distinct Population

Test Number	Complete Sample	Sky Area	Flux Density limit	Frequency GHz	KS statistic	p-value	Significance
1	PR+CJ1	$\delta > 35^\circ, b > 10^\circ$	0.7 Jy	5 GHz	0.34	1.3×10^{-1}	1.1σ
2	PW	$\delta > 10^\circ, b > 10^\circ$	1.5 Jy	2.7 GHz	0.41	3.1×10^{-2}	1.9σ
3	PWS	$10^\circ < \delta < 35^\circ, b > 10^\circ$	1.3 Jy	5 GHz	0.52	1.2×10^{-1}	1.3σ
4	PR+CJ1+PWS	-	-	-	-	1.6×10^{-2}	2.1σ

NOTE—Tests #1 and #3 are independent due to their the different sky areas. We can therefore, legitimately, multiply their p-values, which we do in Test #4. While the results of this redshift test do not rise to the 3σ level, and so cannot be considered to be compelling in and of themselves, they do strongly suggest a difference between most CSO 2s and the rest of the jetted-AGN population, and are therefore supportive of the other tests we present.

The fact that the fraction of CSOs in complete samples is far too high for them all to evolve into larger classes of radio sources was first discussed by R94, and has since been much studied (see OS21). Here we discuss the results for the bona fide CSO 2s in our complete samples. We see from Table 2 that there are 19 CSO 2s and 43 CSS objects in the combined PR+CJ1+PW complete sample. Note that MSOs are a subset of the CSS class. Thus the fraction of CSO 2s in the combined CSO+CSS sample is $(30 \pm 8)\%$. Assuming an upper limit on CSS and MSO sizes of 20 kpc, on our hypothesis of constant speed of advance, the number of CSO 2s in complete samples of CSS and MSOs should be $1/20 = 5\%$. We therefore reject the hypothesis that a significant fraction of CSO 2s evolve into CSS+MSO sources.

The median size of the FR-I sources in the combined PR, CJ1 and PW samples shown in Fig. 1 is 180 kpc. This can be compared to the median size of the CSO 2s in these samples of 215 pc. The ratio in sizes ≈ 837 , so that on the hypothesis of constant expansion speed we would expect there to be $\sim 15,907$ FR Is, whereas there are 16 — i.e., there are $\sim 990\times$ fewer FR Is than

expected. Conversely, given the number of FR Is in these three complete samples, there are $\approx 990\times$ more CSO 2s than expected.

The median size of the FR-II sources in the combined PR, CJ1 and PW samples shown in Fig. 1 is 305 kpc. This can be compared to the median size of the CSO 2s in these samples of 215 pc. The ratio in sizes ≈ 1420 , so that on the hypothesis of constant expansion speed we would expect there to be $\sim 27,000$ FR IIs, whereas there are 77 — i.e., there are $\sim 350\times$ fewer FR IIs than expected. Conversely, given the number of FR IIs in these three complete samples, there are $\approx 350\times$ more CSO 2s than expected.

We see therefore that the numbers of both FR I and FR II sources, relative to CSO 2s are far too small, by factors of over 900 for the FR Is and over 300 for the FR IIs, for CSO 2s to evolve into either FR I or FR II sources of comparable radio luminosity. At this flux density level the integrated number-flux density counts have a power-law slope of -1.3 , so that the luminosity would have to drop by factors of 200 and 90, respectively to accommodate this scenario for FR I or FR II objects.

Rawlings & Saunders (1991) have shown that there is a strong correlation between radio jet power and optical narrow line luminosity. Based on observations by Lawrence et al. (1996), R96 showed that the narrow line luminosities of the CSO 2s J0111+3906, J0713+4349 and J2355+4950 are about a factor 30 below that of typical FR-II galaxies, so that if CSO 2s are to evolve into FR II galaxies, then their optical line luminosities must increase by about a factor 30 while their radio luminosities decrease by about a factor 35, which seems an unlikely scenario. It is interesting to note that R96 show that the jet power for J2355+4950, when corrected for the Hubble constant and different cosmologies, is $\sim 7 \times 10^{43} \text{ erg s}^{-1}$, and for J0111+3906, and J0713+4349 the similarly corrected jet powers $\sim 10^{45} \text{ erg s}^{-1}$, which may be compared to the range of jet powers in FR II sources of $\sim 10^{44} \text{ erg s}^{-1} - 10^{47} \text{ erg s}^{-1}$ (R96). Thus the jet powers of CSO 2s are similar to those of FR II objects, as is also the case regarding their luminosities. Given the agreement in narrow line luminosity between CSO 2s and FR I galaxies, the possible evolutionary scenario from CSO 2s to FR I galaxies may seem promising, but again, the numbers are off by over a factor 900.

We conclude on the basis of these fractions of CSO 2s in complete samples, that the vast majority ($\gtrsim 99\%$) of CSO 2s do not evolve into any of the above classes of larger jetted-AGN, and therefore that they belong to a distinct class of jetted-AGN.

4. THE REDSHIFT DISTRIBUTION OF CSO 2s IN COMPLETE SAMPLES

An independent test of whether or not CSO 2s are drawn from the same population as the other jetted-AGN in our complete samples is provided through the redshift distribution. The redshifts are listed in Table 3. The redshift distributions of the PR+CJ1 and PW complete samples, and their corresponding CSO distributions, are shown in Fig. 2.

We have carried out the Kolmogorov-Smirnov (KS) 2-sample test on the PR+CJ1 sample, the PW sample, and the PWS sample, with the results given in the four tests shown in Table 4. The cumulative distributions corresponding to Tests #1, #2 and #3, and their KS statistics, are shown in Fig. 3 (a), (b) and (c). In carrying out these tests we have removed the CSO 2s from the full samples. The KS statistic is completely determined by the data, but the corresponding p-value depends on the assumptions made in integrating over the parent distribution (Press et al. 1992). We verified that MATLAB and Numerical Recipes use the same formulae for determining the p-values. For that reason we

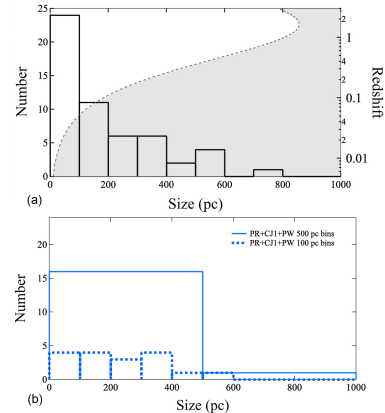


Figure 4. The distributions in size of the bona fide CSOs over the whole CSO size range, from 0 pc to 1 kpc: (a) The heavy black boxes show the histogram of the sample of 54 bona fide CSOs for which there are spectroscopic redshifts, with the numbers given on the left axis. The dashed curve, marking the border of the shaded region, shows the physical size corresponding to 100 milliarcseconds at the redshift indicated on the right-hand axis. For typical VLBI observations at 5 GHz and above, CSOs in the grayed region to the right of this curve would be hard to observe, so there is a strong selection effect that might account for the drop in numbers of bona fide CSOs with physical size. (b) The 17 bona fide CSO 2s with spectroscopic redshifts in the complete flux density-limited PR+CJ1+PW sample. Dotted curves show the data binned into 100 pc bins, while solid curves show the data binned into 500 pc bins. The Kolmogorov-Smirnov and binomial tests both show that this distribution differs from a uniform distribution at the p-value $\sim 1.7 \times 10^{-4}$ (3.6σ) level. While the observed uneven distribution could just be a result of small statistics, it would be foolish to ignore it, especially in light of the corroborating evidence from both the numbers and the redshift distributions. Nature often surprises us.

use the MATLAB p-values in deriving the significance levels in Table 4.

The first two redshift distribution tests (#s 1 and 2 in Table 4) show that the probability of the hypothesis that the CSO 2s and non-CSO 2s are drawn from the same population is 0.13 for the PR+CJ1 sample; and 0.03 for the PW sample. If we look at the effectively complete PW subsample having $S_{5 \text{ GHz}} > 1.3 \text{ Jy}$ and at declination $\delta < 35^\circ$, which is independent of the PR+CJ1 sample in view of the mutually exclusive declination limits, we see that the probability is 0.12. Since these are independent samples, we may legitimately multiply the p-values of Tests #1 and #3, which yields a probability of 1.6×10^{-2} , which is significant at the 2.1σ level. While not at the 3σ level, these statistics nevertheless provide some independent evidence that CSO 2s are drawn from a different population compared to that of the other jetted-AGN in these complete samples.

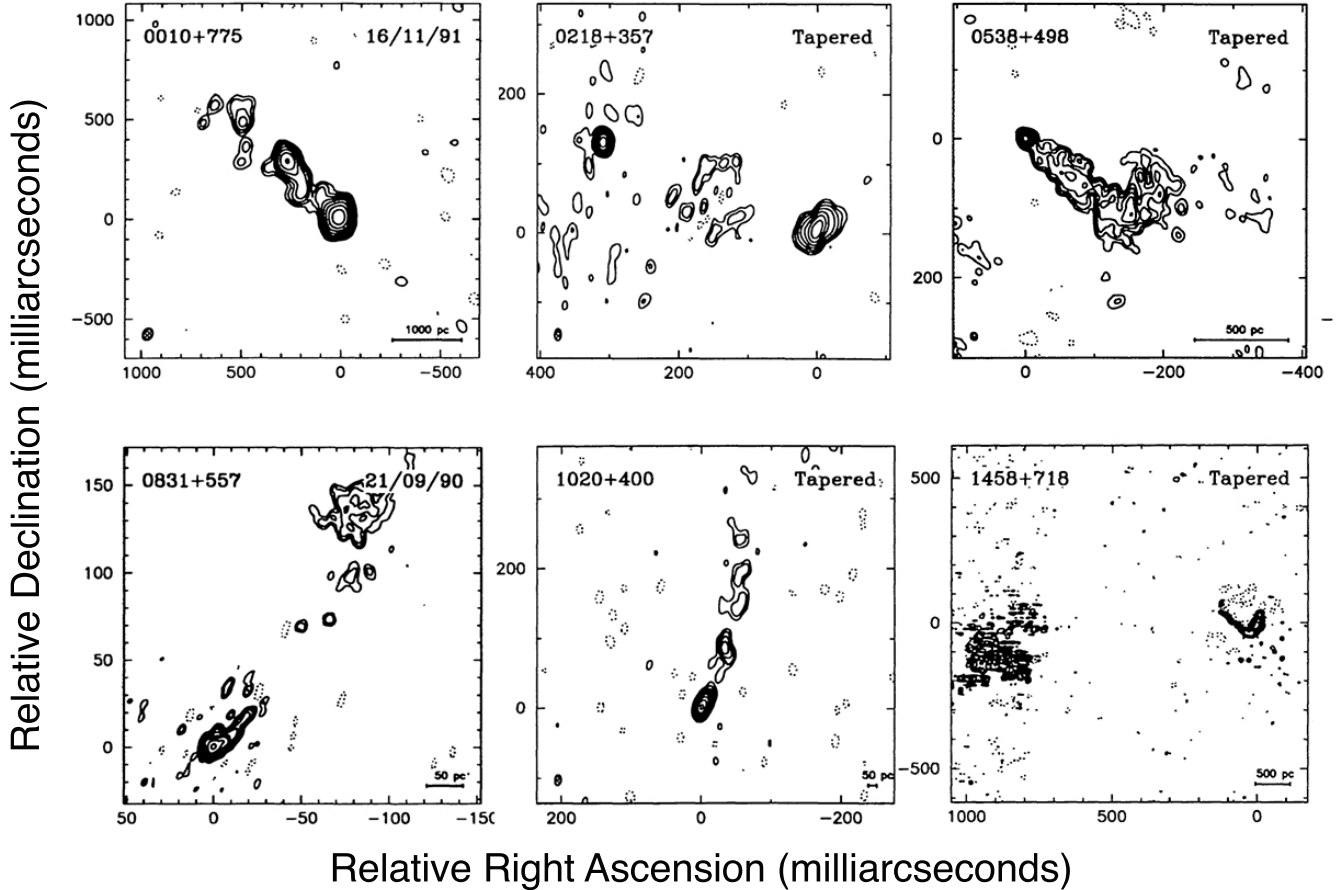


Figure 5. Demonstration that the complete samples studied in this paper are not restricted by the usual ~ 100 milliarcsecond field sizes typical of most VLBI observations at 5 GHz. Shown here are 1.7 GHz VLBI maps of six large angular scale compact AGN from the CJ1 complete sample survey (Polatidis et al. 1995), all of which have sizes $\gg 100$ milliarcseconds. Note that the structure of 1458+718 (J1459+7140, 3C 309.1) extends over 1 arc second — i.e., the map is ten times larger than the typical field of view of VLBI maps at 5 GHz or higher frequencies.

This result, which is seen clearly in the redshift distributions shown in Fig. 2, is interesting. If correct, it suggests that CSO 2s only started forming in significant numbers towards the end of the epoch of maximum galaxy and star formation: The lookback time to the peak in the cosmic star formation rate is ~ 8 billion years (Förster Schreiber & Wuyts 2020), which is close to the lookback time to redshift $z \approx 0.9$, when CSO 2s started to appear in significant numbers, as can be seen in Fig. 2(a) and (b). The peak Star Formation Rate (SFR) occurs from $z \approx 1$ to $z \approx 2$, with the peak Supermassive Black Hole (SMBH) formation rate (Tacconi et al. 2020) peaking slightly after the peak SFR.

Thus, a possible explanation of the origin of CSO 2s is that quiescent SMBHs form CSO 2s by single star capture, and so become significant around $z \sim 1$, when the numbers of both stars and SMBHs in the universe

reach a maximum. We give a detailed discussion of this hypothesis in Paper 3.

However results that are significant only at the $\sim 2\sigma$ level often disappear with the advent of more data, and this particular apparent difference between CSO 2s and other jetted-AGN may disappear as more bona fide CSO 2s are accrued through new and deeper complete samples. An important point that should be mentioned here is that there are 14 bona fide CSOs in the VLBA Imaging and Polarization Survey (VIPS) of flat spectrum ($\alpha \geq -0.5$) sources (Helmboldt et al. 2007) that are not in the complete PR+CJ1+PW samples, and of these only one has redshift greater than 1. Thus, extending the luminosity function almost an order of magnitude deeper appears not to change our findings in this section. This gives us confidence that this preliminary 2.1σ result will be greatly strengthened, when we are able to add the steep spectrum counterparts to the VIPS survey

to make this a complete sample, as we are now engaged in doing.

As a distinct population, and recalling that these are all “short-lived” but not all “young” sources, it will be of great interest to investigate whether CSO 2s show the same strong cosmological evolution as do both high-luminosity extended steep spectrum sources and compact flat spectrum sources (Peacock & Gull 1981), but this is beyond the scope of the present paper.

5. THE SIZE DISTRIBUTION OF CSOs

Our third independent test of the hypothesis that CSO 2s form a distinct class of jetted-AGN is based on the size distribution of CSO 2s. This test is more complex and more subject to selection effects than the tests of the previous two sections. Selection effects are particularly strong when it comes to consideration of the observed distribution of CSO sizes, so we discuss first the effectiveness of our approach in dealing with these selection effects, in order to give the reader some confidence in the statistical robustness of our results.

5.1. *The Efficacy of Complete Samples in Dealing with the CSO Size Distribution Selection Effects*

The distribution of the physical sizes of the 54 bona fide CSO 2s, out of our sample of 79, for which we have spectroscopic redshifts is shown in Fig. 4 (a). It shows a strong cutoff well below 1 kpc. However, one has to bear in mind that this sample of 54 bona fide CSO 2s is a heterogeneous sample gleaned from the literature, and is subject to selection effects. We therefore have to consider carefully whether these selection effects can be eliminated in complete sub-samples of our 54 bona fide CSO 2s.

5.1.1. *The ~ 100 Milliarcsecond Selection Effect*

The first selection effect we consider comes about because the largest angular size that is measured in most cm-wavelength VLBI maps ~ 100 milliarcseconds. In Fig. 4 (a) we show the upper size cutoff this would impose as a function of redshift. Only CSOs to the left of this curve have angular sizes less than 100 milliarcseconds at the corresponding redshift. Clearly this could well impose a strong selection effect on the observed size distribution of CSOs.

On the face of it, it might appear that this selection effect alone is so strong that the true size distribution of CSOs is impossible to determine from these data. Fortunately this is not the case because one can observe complete samples in which one knows the sizes of all the objects in the sample, and if some objects are too large for VLBI mapping at cm wavelengths they can be

observed at longer wavelengths, where the ~ 100 mas limit does not apply. We have availed ourselves fully of this strategy: In addition to the observations of compact objects in the PR+CJ1 complete samples at 5 GHz (Pearson & Readhead 1988; Xu et al. 1995), all of these objects were observed at 1.66 GHz (Polatidis et al. 1995; Xu et al. 1995). In Fig. 5 we show examples of six AGN from the CJ1 complete sample with sizes far exceeding the 100 mas angular size limitation of regular VLBI at 5 GHz and above. As can be seen here, even objects as large as 1 arcsecond were mapped in this survey. This is one of two reasons we can be confident that we have not missed any large CSOs in these complete samples. The other reason is that the large-, by which we mean ($\gtrsim 1$ arcsec), -and small-scale radio structures of *all* of these objects are known. In Table 7 in the Appendix we list references which present the relevant maps of all 281 objects in the PR+CJ1+PW samples.

5.1.2. *Spectral Shape Selection Effect*

Many CSOs are peaked spectrum (PS) sources³. Thus in a sample of CSOs selected at a single frequency, we will clearly include all of the sources that peak at that frequency down to the flux density limit. However, for sources that peak at frequencies significantly higher or lower than the selection frequency, the sample will exclude an increasing number of the CSOs as the separation between the peak frequency and the selection frequency increases. In this study, we therefore consider not only the PR+CJ1 and PW samples, selected at 5 GHz and 2.7 GHz, but we also consider the GLEAM sample, observed using 20 simultaneous flux density measurements spanning frequencies between 72 MHz and 231 MHz, the 3CRR sample selected at 178 MHz, and the Jodrell Bank 966 MHz sample.

The situation is illustrated in Fig. 6. The blue points show the observed radio spectrum of OQ 208 (J1407+2827) (Stanghellini et al. 1997), which has one of the narrowest, most sharply peaked, spectra amongst the bona fide CSO 2s. The gray points illustrate an object with the same spectral shape as OQ 208, but with the maximum shifted from 5 GHz down to 1 GHz, and the peak flux density shifted down to 1.3 Jy. This is the point where the object would drop below the GLEAM 1 Jy limit (Callingham et al. 2017), and the CJ1 700 mJy limit. Because of the drop-off in flux density, relative to the peak, at both higher and lower frequencies, such

³ In this paper we follow the lead of O’Dea & Saikia (2021b) in their comprehensive review of peaked spectrum sources, and refer to GPS and MHz peaked spectrum sources as Peaked Spectrum (PS) sources

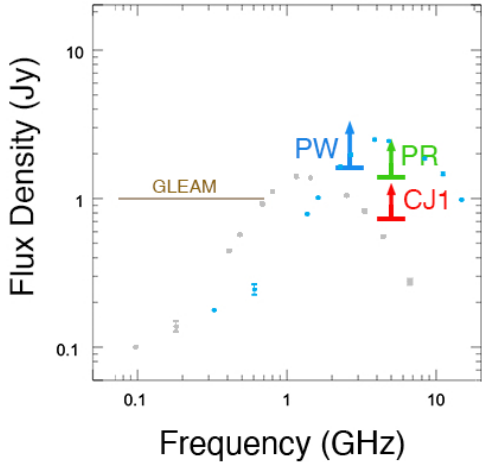


Figure 6. CSO 2s that might be missed in the PR, CJ1, and PW complete samples due to spectral effects: The blue, green and red arrows indicate the selection frequency and limiting flux densities of the PW, PR, and CJ1 samples, respectively. The horizontal brown line indicates the flux density limit of the GLEAM sample. The blue and gray points show the observed spectrum of OQ 208 (Stanghellini et al. 1997), and a shifted spectrum of OQ 208, respectively (see text).

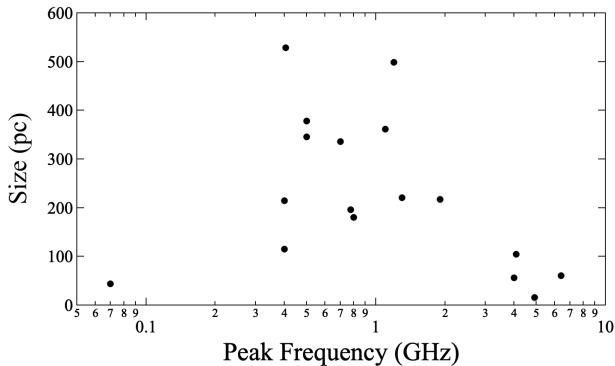


Figure 7. The relationship between size and peak frequency for the CSO 2s in the PR+CJ1+PW complete sample.

an object would not be included in the PW, PR, CJ1 or GLEAM samples. Objects of this type with peak flux densities greater than 1.3 Jy would, however, be included in the GLEAM and CJ1 samples, whose limiting flux densities are indicated by the horizontal brown line in Fig. 6, and the red horizontal bar, respectively. We therefore consider next what is known about the population of objects that peak at frequencies $\lesssim 1$ GHz.

The GLEAM survey covers 72 MHz – 700 MHz, and is concentrated in the southern hemisphere, and so overlaps only part of the sky area covered by the PR+CJ1+PW sample, but it complements the higher frequency VLBI surveys that have studied complete samples because of its lower frequency. 505 of the 11,400 sources in the complete 1 Jy GLEAM sample ($(4.4 \pm 0.2) \%$) are peaked-spectrum objects (Callingham et al. 2017), with peak flux densities above 1 Jy in the 72 MHz – 700 MHz range, and so must also be compact (Readhead et al. 2021). Similarly, in a LOFAR study of northern radio sources at 150 MHz, Slob et al. (2022) found 373 PS sources and concluded that $\sim 2.5\%$ of sources in complete samples around 150 MHz are PS sources. We note the similarity in the fractions of PS sources identified in the LOFAR (150 MHz), GLEAM (72 MHz - 700 MHz), and the fraction of PW+CJ1+PW (2.7 GHz and 5 GHz) CSO 2s samples, which are $\sim 2.5\%$, $\sim 4.4\%$, and $\sim 6.8\%$, respectively. It is possible that a significant fraction of the PS population in both the LOFAR and GLEAM surveys are CSO 2s, and thus that there is a significant population of CSO 2s extending to below 100 MHz. In this case we could well be missing CSO 2s that could fall into in the 500 pc – 1 kpc size range. In Fig. 7 we show the sizes of the PR+CJ1+PW CSO 2s plotted against peak frequency. It is interesting to note that almost half of these objects have peak frequencies in the range covered by the GLEAM survey, even though they were selected at 2.7 GHz and/or 5 GHz. It is also interesting to note that, apart from the small fraction ($< 25\%$) that has peak frequencies above 3 GHz, there is no clear dependence of size on frequency.

5.2. A Spectral Shape Lacuna

As we have seen in previous sections, we are only considering the 17 bona fide CSO 2s in the PR+CJ2+PW complete sample with known spectroscopic redshifts, and there are only two bona fide CSOs in these complete samples without a spectroscopic redshift. The PR+CJ2+PW complete sample, excluding M82, consists of the 281 sources listed in Table 7, including M82. In 5.1.2 we discussed a spectral shape selection effect that can be affecting this sample. The GLEAM survey detected 11,400 sources with flux densities greater than 1 Jy between 70 MHz and 700 MHz. Of these 505 are PS sources. In order to double the numbers of CSO 2s, and hence potentially to have a strong effect on any statistical tests of the size distribution of CSO 2s, there would need to be ≈ 17 bona fide CSO 2s in the GLEAM sample. Thus only a small fraction $\sim 3\%$ (17/505) of the PS sources in the GLEAM would need to be CSO 2s

in order potentially to have a significant impact on the statistics. So this is a lacuna that has to be addressed in any size tests.

In the next three subsections we advance two independent arguments to address this lacuna and we suggest a test that could fill the lacuna, but which requires more observations and is therefore beyond the scope of the present paper.

5.2.1. *The Range of Peak Frequencies in Our Sample*

In Paper 1, Fig. 6, we have plotted the range of peak frequencies observed, and it can be seen that the peak frequencies range from below 80 MHz to ~ 10 GHz. The same is true of the objects in our combined PR+CJ1+PW sample - the lowest peak is at 70 MHz and the highest peak is at 6.4 GHz, and the distribution of the peaks is roughly uniform between these extremes.

Thus the selection procedure of the complete PR+CJ1+PW sample and our bona fide CSO identification method do not appear to have created a bias against CSO 2s peaking anywhere within this range. However, while the (rarer) flat-spectrum CSO 2s will not suffer from the spectral selection biases described earlier, some peaked-spectrum CSO 2s could be excluded from the sample for certain redshift ranges. This could, therefore, influence the size distribution of the observed CSO 2s in the PR+CJ1+PW samples, particularly if CSO intrinsic size is related to peak frequency and/or luminosity.

In the next two subsections we give an argument that shows that spectral shape selection effects are unlikely to have biased the size distribution of the CSO 2s in the PR+CJ1+PW sample.

5.2.2. *The 3CRR and PW CSS Double Sample*

In addition to our complete samples of CSO 2s, described in the previous sections, there is one other relevant sample of CSO 2s and MSOs that has been studied extensively by the Bologna Group (BG), the key results of which are given in a series of papers (Fanti et al. 1985, 1990; Spencer et al. 1991; Fanti et al. 1995; Dallacasa et al. 1995, 2013, 2021). The BG identified 32 double-lobed CSS objects, given in Table 1 of Fanti et al. (1995), in their sample drawn from the 3CRR (Laing et al. 1983) and the PW samples. They subsequently added one double-lobed source (1819+396 = 4C +39.56) that they had previously missed (Dallacasa et al. 2021), bringing the total of double-lobed CSS sources in the BG sample to 33. Given that these are CSS objects, they excluded flat spectrum objects with $\alpha > -0.5$.

This spectral filter against flat spectrum sources ($\alpha > -0.5$), as applied to the 3CRR sample, which has a limiting flux density of 10 Jy at 178 MHz, excludes sources

brighter than 2.57 Jy at 2.7 GHz. Since these are greater than the flux density limit of the PW complete sample (1.5 Jy at 2.7 GHz), any such object can be included in the BG study by adding the flat spectrum PW CSO 2s to the steep spectrum CSO 2s detected by the BG, in order to get the total of both flat and steep spectrum compact doubles, including CSO 2s, in the 3CRR and PW samples (note that there are no flat spectrum doubles of size greater than 1 kpc in PW). There are four BG CSOs in our sample of 79 bona fide CSOs listed in Paper 1. All four of these BG CSOs are already in our complete sample of CSOs in the PR+CJ1+PW complete samples.

We therefore compensate for the spectral index limit in BG sample by adding the flat spectrum PW bona fide CSO 2s that were excluded from the BG sample by the spectral index cutoff at $\alpha = -0.5$ to the BG sample of CSO 2s, thereby making this into a complete sample of 3CRR+PW compact double sources, and bringing the total including the PW flat spectrum CSO 2s to 40. In order to apply the same largest angular size filter as that used in Paper 1, we have re-measured the largest angular sizes of the 33 BG CSS double sources at the lowest frequency at which high-quality maps are available in the BG group's publications listed above. The results are shown in Fig. 8, together with the 7 flat spectrum PW bona fide CSO 2s that we have added.

We find that 27 of the 33 objects in the BG sample fit the CSO+MSO criteria, with four of the objects being bona fide CSO 2s and the remaining 23 objects being MSOs. The 6 remaining objects all have largest projected physical sizes greater than 20 kpc, based on our measured largest angular sizes. When we add the flat spectrum objects from the PW sample, the number of CSO 2s increases from 4 to 11, as shown in Fig. 8.

The four CSO 2s in the BG CSS sample all have sizes between 300 pc and 500 pc. These PS CSO 2s have spectral turnovers that are almost certainly due to synchrotron self absorption as is shown in the paper by Scott & Readhead (1977), who showed that the equipartition angular size $\psi_{\text{eq}} \propto S_{17}^{\frac{8}{17}} \nu^{-\frac{35+2\alpha}{34}} (1+z)^{\frac{15-2\alpha}{34}}$. Thus fainter objects that show spectral peaks at higher frequencies will be smaller than the four CSS CSO objects in the BG sample. It therefore is unlikely that there will be a significant number of CSS CSO 2s with sizes in the 500 pc to 1 kpc range. We return to this point in §5.3.

5.2.3. *The Jodrell Bank 966 MHz Sample*

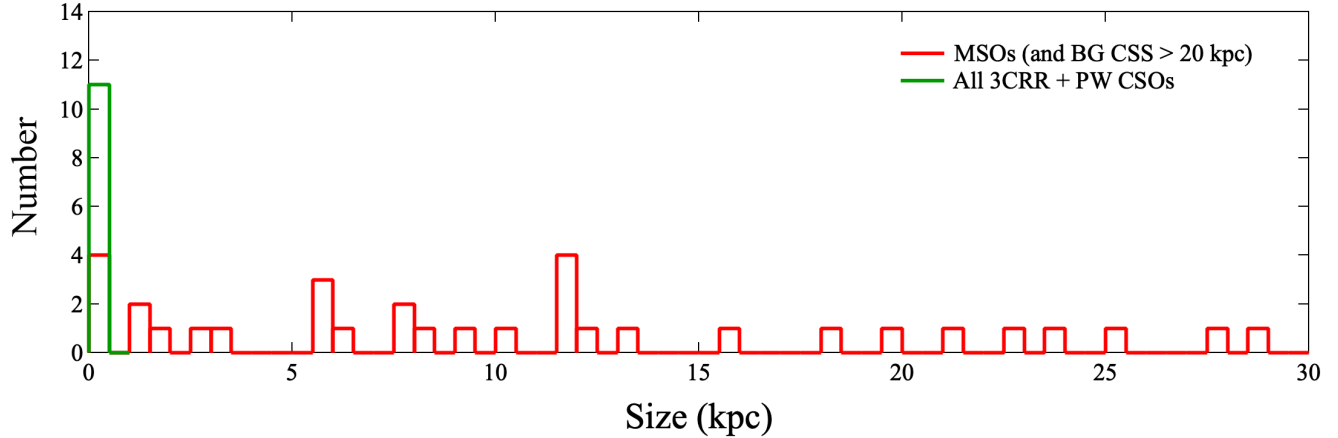


Figure 8. The distributions of the bona fide CSO 2s and MSOs as a function of projected physical size in the BG sample. The red distribution shows the BG CSO 2s+MSOs+CSS>20 kpc objects. The green distribution shows the BG+PW CSO 2s.

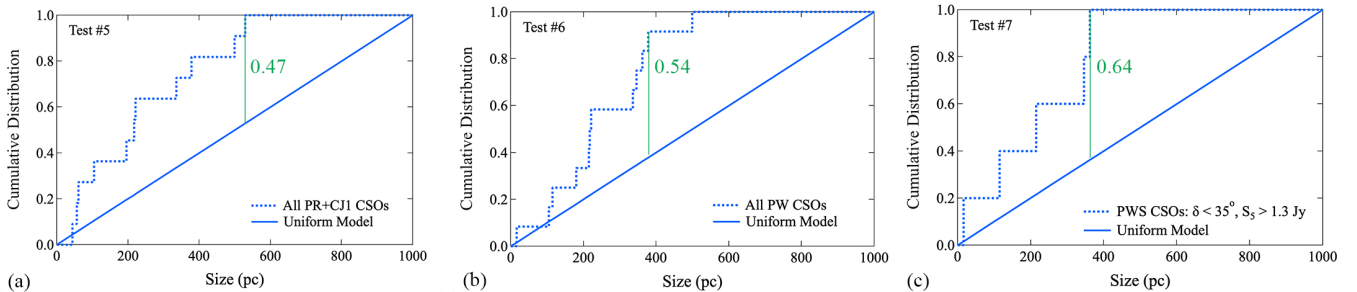


Figure 9. KS Tests on the size distributions of the bona fide CSO 2s in the PR+CJ1 and PW samples. (a), (b) and (c): comparison of the CSO 2 cumulative size distributions *vs.* the uniform model for the PR+CJ1, PW, and PWS samples, respectively. The green bars indicate the maximum differences in the cumulative distributions, corresponding to the values of the KS statistic given by the numbers in green. The corresponding p-values are listed in Table 5.

Since the 3CRR sample is complete down to 10 Jy at 178 MHz (Laing et al. 1983), for comparison with the other samples in this study it would be helpful to have a low frequency sample complete down to ~ 1 Jy. Fortunately, such a sample exists for which the radio structures of over 98% of the objects are known.

Referring back to Fig. 6 and the objects in the lacuna illustrated by the gray spectrum. We can define a complete sample drawn from the Jodrell Bank 966 MHz survey (Cohen et al. 1977), which produced a radio catalogue and measured arcsec-level positions for the majority of its sources. We have selected a sub-sample, consisting of 169 of the strongest sources ($S_{0.966} > 1.5$ Jy) from Cohen et al. (1977). This sub-sample is unbiased, and while the full survey is not strictly complete due to confusion issues, these apply only at low flux density levels, and thus the sub-sample that we have selected is not affected by confusion. We will refer to this unbiased sub-sample of 169 objects as the “JBS” sample.

We classified 74 of the JBS sample in the filtering process we carried out in selecting our bona fide CSO 2s described in Paper 1. We identified six of them as bona fide CSO 2s.

We have extracted VLASS cutout images of all 169 JBS objects using the CIRADA cutout server⁴, and we found only 17 of them to be unresolved, with largest angular size < 3 arc sec, and hence possible CSO 2s. Of these 17 compact objects, two are MOJAVE “core-jet” objects, and one is a 2 arc second double. Thus there are 14 possible CSO 2s in the 966 MHz JBS sample in addition to the 6 bona fide CSO 2s we have already identified. We are engaged in obtaining VLBI observations of these 14 objects.

5.3. Statistical Analysis of CSO Sizes in the Complete Samples

⁴ <http://cutouts.cirada.ca>

Table 5. One-sample KS Tests Against a Uniform Distribution of CSO 2 Sizes

Test Number	Complete Sample	Sky Area	Flux Density limit	Frequency GHz	KS statistic	p-value	Significance
5	PR+CJ1	$\delta > 35^\circ, b > 10^\circ$	0.7 Jy	5 GHz	0.47	9.3×10^{-3}	2.4σ
6	PW	$\delta > 10^\circ, b > 10^\circ$	1.5 Jy	2.7 GHz	0.54	8.7×10^{-4}	3.1σ
7	PWS	$10^\circ < \delta < 35^\circ, b > 10^\circ$	1.3 Jy	5 GHz	0.64	1.7×10^{-2}	2.1σ
8	PR+CJ1+PWS	-	-	-	-	1.6×10^{-4}	3.6σ

NOTE—Tests of the observed CSO 2 size distribution compared to a uniform size distribution. The PWS sample is the effectively complete subsample of the PW sample having $10^\circ < \delta < 35^\circ, |b| > 10^\circ$ and $S_{5\text{ GHz}} \geq 1.3\text{ Jy}$ (see text).

Table 6. Binomial Tests of Significance Levels of CSO Size Distributions in Complete Samples

Test Number	Complete Sample	Sky Area	α limit	N 0 – 500 pc	N 500 pc-1 kpc	p-value	Significance
9	PR+CJ1	$\delta > 35^\circ, b > 10^\circ$	-	11	1	5.4×10^{-3}	2.6σ
10	PWS	$\delta < 35^\circ, b > 10^\circ$	-	6	0	3.1×10^{-2}	1.9σ
11	PR+CJ1+PWS	-	-	-	-	1.7×10^{-4}	3.6σ

NOTE— The PR+CJ1 and PWS ($\delta < 35^\circ, S_5 > 1.3\text{ Jy}$) samples are independent, so we have multiplied their p-values in Test 11 (see text).

As we have seen, all of the bona fide CSOs in the complete PR, CJ1 and PW samples are CSO 2s — i.e., as discussed in Paper 1, they are edge-brightened, high-luminosity objects. This is a selection effect resulting from the flux density limits in the complete samples. The size distribution of the CSO 2s in the PR+CJ1+PW complete sample is shown in Fig. 4(b), binned into 100 pc and 500 pc intervals.

Using the CSO 2 size distributions in the PR+CJ1 and PW complete samples, we have carried out two sets of statistical tests of the hypothesis that CSO 2s are uniformly distributed in size between 0 pc and 1000 pc, as would be expected on the hypothesis that the speed of advance is constant: (i) a set of KS 1-sample tests, which yield the cumulative distributions shown in Fig. 9 (a), (b) and (c) and the p-values shown in Tests #5 - #8 in Table 5; and (ii) binomial tests in which we divided the CSO 2s into two size bins, from 0 pc to 500 pc, and from 500 pc to 1000 pc, which yield the results shown in Table 6.

We consider first the KS tests shown in Table 5. We see there that the uniform hypothesis is rejected by the PR+CJ1 CSO sample at the 9.3×10^{-3} probability level, and by the PW CSO sample at the 8.7×10^{-4} probability level. The independent, effectively complete, PW

CSO sample below declination 35° (Test #7) rejects the uniform hypothesis at the 1.7×10^{-2} level.

Tests #5 and #7 are independent – note the different sky areas – and at the same observing frequency. We can therefore, legitimately, multiply their p-values. This gives Test #8, which rejects the uniform size distribution hypothesis at the p-value 1.6×10^{-4} , or 3.6σ significance level.

The results of the binomial tests, shown in Table 6, show that by similarly combining the PR+CJ1 CSO sample (Test #9) with the independent PWS sample (Test #10), as shown in Test #11, the uniform hypothesis is rejected at the 1.7×10^{-4} (3.6σ) level.

In our view, these tests on complete samples constitute compelling evidence that the size distribution of CSO 2s cuts off sharply at ≈ 500 pc, which is significantly below the 1 kpc size limit imposed by the defining criteria of CSOs. As described in §5.2.3, the existence of this sharp cutoff can be tested, for example, with MERLIN and VLBI observations of the 14 potential CSO 2s in the complete JBS sample.

Clearly *some* CSO 2s must grow to larger sizes in order to produce MSOs. An example of a CSO and MSO with remarkably similar morphologies is shown in Fig. 10, which illustrates this point, especially since 0404+768 (J0410+7656) was originally classified as a CSO, but

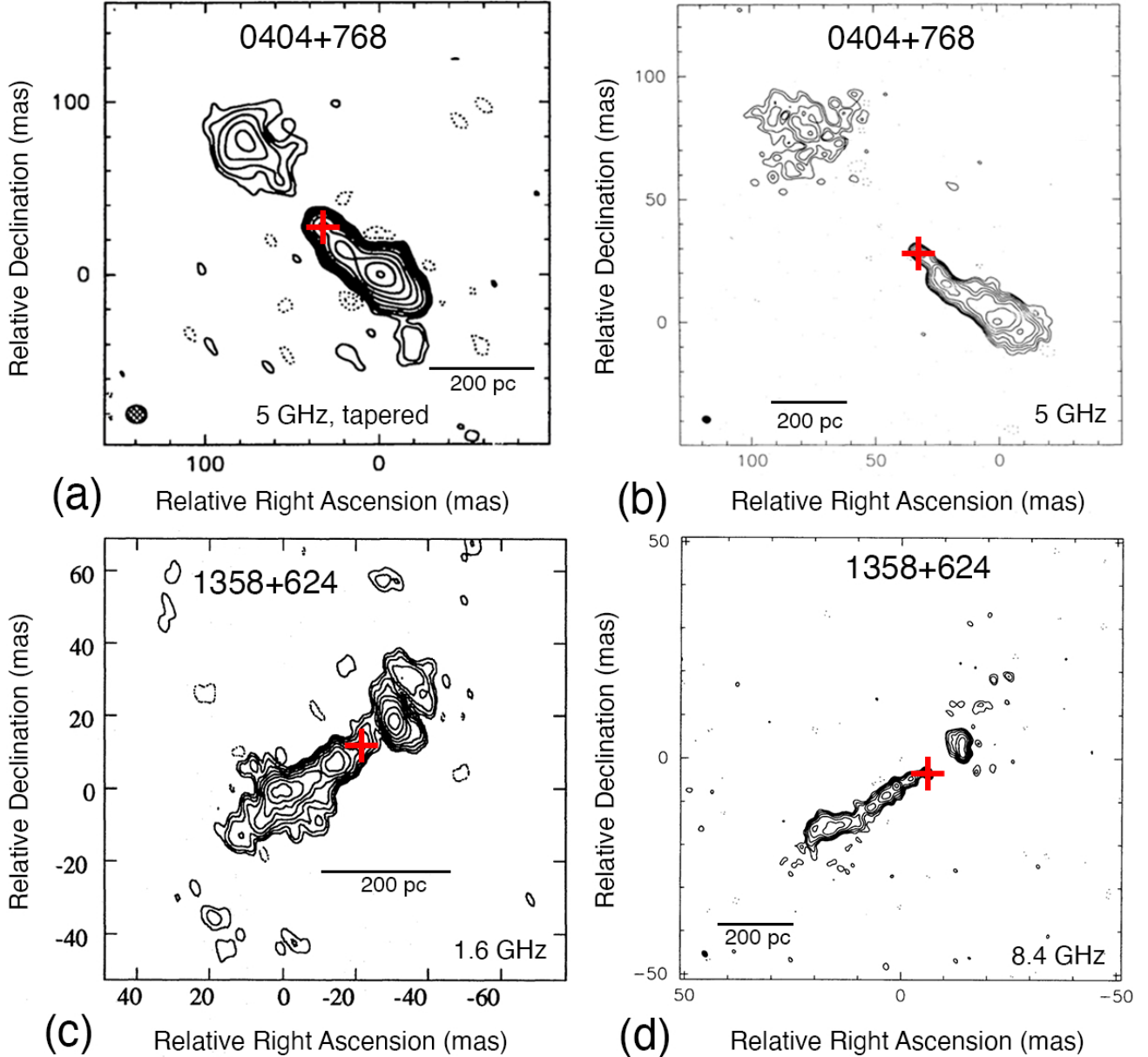


Figure 10. Example of an MSO and a CSO, with similar morphologies. The MSO:(a) from Xu et al. (1995), and (b) from Taylor et al. (1996): 0404+768 (J0410+7656), which these authors had classified as a CSO. The CSO: from Dallacasa et al. (1995), and (d) from Taylor et al. (1996): 1358+624 (J1400+6210). Some CSO 2s must evolve into MSOs, and 1358+624 may be just such a case. The red cross marks the location of the core in each map.

fails the size cutoff (by $\sim 20\%$). It is clear that the majority of CSO 2s do not grow much above 500 pc in projected size.

6. RESULTS AND TESTS FROM THIS PAPER

The results and tests that have come out of this study are listed below.

6.1. Results

The number fraction, redshift, and size statistics discussed in the previous three sections and presented in Tables 4 to 6 demonstrate that (i) most CSO 2s are drawn from a population of jetted-AGN that is distinct from other jetted-AGN, and (ii) the size distribution of CSO 2s cuts off sharply at ≈ 500 pc, a finding that is verifiable (see §5.2.3).

These are significant findings. They show that there has to be something fundamentally different between

CSO 2s and the larger sources. While both must be driven by the same type of central engine, since both are producing high-luminosity relativistic jets, there must be some fundamental difference between them to produce two such different outcomes – one with a size cutoff around 500 pc and the other with a size cutoff $\sim 200\times$ larger.

One might think, for example, that the cutoff could be explained simply by random episodic fuelling. But how would random episodic fuelling produce a sharp cutoff? Random episodic fuelling would produce a uniform distribution. There has to be another explanation for the cutoff, such as, for example, an upper limit on the size of the fuel packages, a change in the jet environment that leads the jets to fade beyond a certain distance from the central engine, or a mechanism associated with the accretion disk that limits the energy of the jet.

6.2. Tests

The major tests resulting from this paper are the following:

1. We will follow-up the JBS sample with MERLIN and VLBA observations in order to test the sharp cutoff in size we have seen in the PR+CJ1+PW complete sample.
2. We have undertaken a program to increase the number of CSO 2s in complete samples by a factor of at least 3, to ~ 50 by carrying out a VLBI survey of ~ 332 steep spectrum sources that complement the VIPS flat spectrum survey, thus converting VIPS into a complete sample. This will further test the cutoff in CSO 2 size distribution.
3. Structural studies of the PS objects identified in the LOFAR and GLEAM surveys would be well worth doing.

7. DISCUSSION

Although the selection effects inherent in our literature search for CSOs are significant, we have shown that, with careful use of complete samples, and using the 17 CSO 2s in the complete PR, CJ1, and PW samples for which we have spectroscopic redshifts, it is possible to carry out a series of rigorous statistical tests that provide what we regard as compelling evidence that the vast majority of CSO 2s constitute a population of jetted-AGN that is distinct from, and therefore requires a separate origin to, the larger classes of jetted-AGN, such as CSS sources, MSOs, and FR I and FR II objects.

The physical size cutoff is clearly telling us something important about this class of jetted-AGN. The scenario that produces almost all CSO 2s must be different in some important way from that which produces the larger

symmetric radio sources. We return to this discussion of the origins of CSO 2s in Paper 3.

It should be clear, therefore, that, (i) because the observed emission regions in these objects are not significantly relativistically boosted towards the observer, thereby making it possible to determine their detailed physical properties, and (ii) most CSO 2s belong to a distinct class of jetted-AGN, these CSO 2s provide a unique time domain plus structural window on the central engines of jetted-AGN and the supermassive black holes that drive them.

We thank John Peacock for useful discussions. We thank the reviewer of this paper for many helpful suggestions that have clarified several important aspects of this work. We are grateful for the use of the CATS database of Verkhodanov et al. (2005), of the Special Astrophysical Observatory. This research has made use of NASA's Astrophysics Data System Bibliographic Services. This research has made use of the NASA/IPAC Extragalactic Database (NED) which is operated by the Jet Propulsion Laboratory, California Institute of Technology, under contract with the National Aeronautics and Space Administration. This research has made use of data from the OVRO 40-m monitoring program (Richards, J. L. et al. 2011, ApJS, 194, 29), supported by private funding from the California Institute of Technology and the Max Planck Institute for Radio Astronomy, and by NASA grants NNX08AW31G, NNX11A043G, and NNX14AQ89G and NSF grants AST-0808050, AST-1109911, and AST-1835400. This research has made use of data from the MOJAVE database that is maintained by the MOJAVE team (Lister et al. 2018). The MOJAVE program is supported by NASA-*Fermi* grant 80NSSC19K1579. This research has made use of the CIRADA cutout service at <http://cutouts.cirada.ca>, operated by the Canadian Initiative for Radio Astronomy Data Analysis (CIRADA). CIRADA is funded by a grant from the Canada Foundation for Innovation 2017 Innovation Fund (Project 35999), as well as by the Provinces of Ontario, British Columbia, Alberta, Manitoba and Quebec, in collaboration with the National Research Council of Canada, the US National Radio Astronomy Observatory and Australia's Commonwealth Scientific and Industrial Research Organisation. S.K. and K.T. acknowledge support from the European Research Council (ERC) under the European Unions Horizon 2020 research and innovation programme under grant agreement No. 771282. KT acknowledges support from the Foundation of Research and Technology - Hellas Synergy Grants Program through project POLAR, jointly implemented by the Institute of Astrophysics and the Institute of Computer Science. A.S. was supported by the NASA Contract NAS8-03060 to the Chandra X-ray Center.

This paper depended on a very large amount of VLBI data, almost all of which was taken with the Very Long Baseline Array. The National Radio Astronomy Observatory is a facility of the National Science Foundation operated under cooperative agreement by Associated Universities, Inc.

Table 7. Structure Types and Literature References for the Combined PR, CJ1 and PW[†] Samples

B1950 Name	J2000 Name	Alias	PR	CJ1	PW	Type	Optical ID [‡]	Large-scale Structure	Small-scale Structure
(1)	(2)	(3)	(4)	(5)	(6)	(7)	(8)	(9)	(10)
0010+775	J0013+7748	S5 0010+77		Y		CT,CSS	G		41,42
0010+405	J0013+4051	4C +40.01		Y		CT,CFS	G		41,42
0013+790	J0016+7916	3C 6.1		Y	Y	FR II	G	3,9,62	
0016+731	J0019+7327	S5 0016+73	Y		Y	U,CFS	Q	9	31
0022+390	J0025+3919	S4 0022+39		Y		CT,CFS	Q		41,42
0026+34	J0029+3456	B2 0026+34			Y	CSO	G		58, 67
0038+32	J0040+3310	3C 19			Y	FR II	G	8,9,62	
0040+517	J0043+5203	3C 20	Y		Y	FR II	G	8,9,64	
0048+509	J0050+5112	3C 22.0		Y		FR II	G	8	
0102+480	J0105+4819			Y		CT,CFS			41,42
0104+32	J0107+3224	3C 31			Y [†]	FR I	G	8,9	
0106+13	J0108+1320	3C 33			Y [†]	FR II	G	9,34	
0106+729	J0109+7311	3C 33.1		Y	Y	FR II	G	8,9	
0108+388	J0111+3906	S4 0108+388	Y			CSO	G	66	31, 41
0116+31	J0119+3210	4C 31.04			Y [†]	CSO	G		35, 68
0123+32	J0126+3313	3C 41			Y [†]	FR II	G	5,9,62	
0125+28	J0128+2903	3C 42			Y	FR II	G	8,9	
0127+23	J0129+2338	3C 43			Y	CSS	Q	9,48	
0133+20	J0136+2057	3C 47			Y	FR II	Q	3,9	
0133+476	J0136+4751	OC 457	Y		Y	U,CFS	Q	9	31
0134+32	J0137+3309	3C 48			Y [†]	CSS	Q	9,48	
0138+13	J0141+1353	3C 49			Y	CSS	G	9,48	
0153+744	J0157+7442	S5 0153+744	Y		Y	U,CFS	Q	9	31
0202+14	J0204+1514	4C 15.05			Y [†]	U,CFS	Q ^a	9	58
0206+355	J0209+3547	4C +35.03		Y		FR I	G	3	
0212+735	J0217+7349	S5 0212+73	Y		Y	U,CFS	Q	9	31
0218+357	J0221+3556	B2 0218+357		Y		CT,CFS	Q		41,42
0210+860	J0222+8619	3C 61.1	Y		Y	FR II	G	9,34	
0220+427	J0223+4259	3C 66B	Y		Y	FR I	G	9,46	
0220+397	J0223+4000	3C 65		Y	Y	FR II	G	5,9	
0221+27	J0224+2750	3C 67			Y	CSS	G	9,48	
0223+34	J0226+3421	4C 34.07			Y [†]	CSS	Q ^a	9,57,56	
0235+16	J0238+1636	PKS 0235+164			Y [†]	U,CFS	Q	9	58
0248+430	J0251+4315	B3 0248+430		Y		CT,CFS	Q		41,42
0258+350	J0301+3512	NGC 1167		Y		FR I	G	28	
0300+16	J0303+1626	3C 76.1			Y [†]	FR I	G	9,34	
0307+16	J0310+1705	3C 79			Y [†]	FR II	G	9,23,62,64	

Table 7 *continued*

Table 7 (*continued*)

B1950 Name	J2000 Name	Alias	PR	CJ1	PW	Type	Optical ID [‡]	Large-scale Structure	Small-scale Structure
(1)	(2)	(3)	(4)	(5)	(6)	(7)	(8)	(9)	(10)
0307+444	J0310+4435	4C 44.07		Y		CSS	Q	53	
0309+390	J0312+3916	4C 39.11		Y		CT,CSS	G		59
0314+416	J0318+4151	3C 83.1B	Y		Y	FR I	G	6,9	
0316+16	J0318+1628	CTA 21			Y [†]	CSS	G	9	58
0316+413	J0319+4130	3C 84	Y		Y	U,CFS	G	9,33	61,56
0319+12	J0321+1221	PKS 0319+12			Y	CSS	Q ^a	9	54,56
0356+10	J0358+1026	3C 98			Y [†]	FR II	G	9,47	
0400+25	J0403+2600	CTD 26			Y [†]	U,CFS	Q	9	58
0402+379	J0405+3803	4C +37.11		Y		CSO	G		41,42
0404+768	J0410+7656	4C 76.03	Y		Y	CSS	G	9,57	56
0407+747	J0413+7451	4C 74.08		Y	Y	FR II	G?	9,19	
0410+11	J0413+1112	3C 109			Y [†]	FR II	G	9,39	
0411+14	J0414+1416	4C 14.11			Y	FR II	G	9,34,64	
0428+20	J0431+2037	PKS 0428+20			Y [†]	U,CFS	G ^a	9	54,56
0433+29	J0437+2940	3C 123			Y [†]	FR II	G	9,52,62,64	
0453+22	J0456+2249	3C 132			Y	FR II	G	8,9,62,64	
0454+844	J0508+8432	S5 0454+84	Y			CT,CFS	Q		31
0518+16	J0521+1638	3C 138			Y [†]	CSS	Q	9,48	57
0528+13	J0530+1331	PKS 0528+134			Y [†]	U,CFS	Q ^a	9	58
0538+498	J0542+4951	3C 147	Y		Y	CSS	Q	9,48	
0602+673	J0607+6720			Y		CT,CFS	Q		41,42
0605+480	J0609+4804	3C 153	Y		Y	FR II	G	3,9,62,64	
0620+389	J0624+3856	S4 0620+389		Y		CT,CFS	Q		41,42
0615+820	J0626+8202	S5 0615+82		Y		CT,CFS	Q		58
0642+449	J0646+4451	OH 471		Y		CT,CSS	Q		41,42
0646+600	J0650+6001	4 0646+60		Y		CT,CFS	Q		41,42
0650+371	J0653+3705	S4 0650+371		Y		CT,CFS	Q		41,42
0651+542	J0655+5408	3C 171		Y	Y	FR II	G	9,49,64	
0703+426	J0706+4230	4C 42.23		Y	Y	FR I	G	9,19	
0702+749	J0709+7449	3C 173.1		Y		FR II	G	34	
0707+476	J0710+4732	S4 0707+47		Y		CT,CFS	Q		41,42
0707+689	J0713+6852	4C 68.08		Y		CSS	Q	45	
0710+439	J0713+4349	B3 0710+439	Y		Y	CSO	G		31, 69
0711+356	J0714+3534	OI 318	Y		Y	U,CFS	Q	9	31
0716+714	J0721+7120	TXS 0716+714		Y		CT,CFS	Q		41,42
0723+679	J0728+6748	3C 179	Y		Y	FR II	Q	9,19,62	
0735+17	J0738+1742	OI 158			Y [†]	U,CFS	Q	9	58
0738+31	J0741+3112	OI 363			Y [†]	U,CFS	Q	9	58
0734+805	J0743+8026	3C 184.1		Y	Y	FR II	G	9,47	

Table 7 (*continued*)

Table 7 (continued)

B1950 Name	J2000 Name	Alias	PR	CJ1	PW	Type	Optical ID [‡]	Large-scale Structure	Small-scale Structure
(1)	(2)	(3)	(4)	(5)	(6)	(7)	(8)	(9)	(10)
0742+10	J0745+1011	OI 471			Y [†]	U,CFS	EF ^a	9	58
0744+55	J0748+5548	DA 240			Y	FR ?	G	9,24	
0746+483	J0750+4814	S4 0746+483		Y		CT,CFS	Q		41,42
0748+12	J0750+1231	OI 280			Y [†]	U,CFS	Q	9	58
0740+828	J0750+8241	S5 0740+82		Y		CT,CSS	Q		41,42
0755+379	J0758+3747	NGC 2484		Y	Y	CSS	G	9	41,42
0802+24	J0805+2409	3C 192			Y [†]	FR II	G	9,47	
0804+499	J0808+4950	OJ 508	Y		Y	U,CFS	Q	9	31
0805+410	J0808+4052	S4 0805+41		Y		CT,CFS	Q		41,42
0809+483	J0813+4813	3C 196	Y		Y	FR II	Q	9.25	
0812+367	J0815+3635	B2 0812+36		Y		CT,CFS	Q		41,42
0814+425	J0818+4222	OJ 425	Y		Y	U,CFS	Q	9	31
0816+526	J0819+5232	4C 52.18		Y		FR II	G	13	
0818+472	J0821+4702	3C 197.1		Y		FR II	G	4,9,62	
0820+560	J0824+5552	OJ 535		Y		CT,CFS	Q		41,42
0821+394	J0824+3916	4C +39.23		Y		CT,CFS	Q		41,42
0827+378	J0831+3742	B2 0827+37		Y		CT,CSS	Q		41,42
0828+493	J0832+4913	OJ 448		Y		CT,CFS	Q		41,42
0831+557	J0834+5534	4C 55.16	Y		Y	U,CFS	G	9	31
0833+585	J0837+5825	S4 0833+58		Y		CT,CFS	Q		41,42
0838+13	J0840+1312	3C 207			Y [†]	FR II	Q	3,9,62	
0836+710	J0841+7053	4C 71.07	Y		Y	U,CFS	Q ^a	9	31
0844+540	J0847+5352	NGC 2656		Y		FR I	G	12	
0850+581	J0854+5757	4C 58.17	Y			CT,CFS	Q		31
0851+20	J0854+2006	OJ 287			Y [†]	U,CFS	Q	9	58
0859+470	J0903+4651	4C 47.29	Y		Y	U,CFS	Q	9	n,31
0900+428	J0904+4238	B3 0900+428		Y		CT,CFS	G		41,42
0906+430	J0909+4253	3C 216	Y		Y	U,CFS	Q	9,48,62	31
0917+449	J0920+4441	TXS 0917+449		Y		CT,CFS	Q		41,42
0917+458	J0921+4538	3C 219	Y		Y	FR II	G	9,36	
0917+624	J0921+6215	OK 630		Y		CT,CFS	Q		41,42
0923+392	J0927+3902	4C 39.25	Y		Y	U,CFS	Q	9	60
0936+361	J0939+3553	3C 223		Y	Y	FR II	G	9,47	
0938+399	J0941+3944	3C 223.1		Y		Complex	G	50	
0939+14	J0942+1345	3C 225B			Y	FR II	G	8,9	
0945+408	J0948+4039	4C 40.24	Y			CT,CFS	Q		31
0945+664	J0949+6615	4C 66.09		Y	Y	U,CFS	G	9	41,42
0945+73	J0949+7314	4C 73.08			Y	FR II	G	7	
0947+14	J0950+1420	3C 228			Y	FR II	G	8,9,62	

Table 7 continued

Table 7 (continued)

B1950 Name	J2000 Name	Alias	PR	CJ1	PW	Type	Optical ID [†]	Large-scale Structure	Small-scale Structure
(1)	(2)	(3)	(4)	(5)	(6)	(7)	(8)	(9)	(10)
0951+699	J0955+6940	M82* (3C 231)	Y		Y	FR ?	G	9,10	
0954+556	J0957+5522	4C 55.17	Y		Y	U,CFS	Q	9	31
0955+476	J0958+4725	OK 492		Y		CT,CFS	Q		41,42
0954+658	J0958+6533	S4 0954+65	Y			CT,CFS	Q		58
0958+29	J1001+2847	3C 234			Y [†]	FR II	G	9,29,64	
1003+351	J1006+3454	3C 236	Y		Y	FR II	G	9,24	
1003+830	J1010+8250	S5 1003+83		Y		CT,CFS	G		41,42
1007+416	J1010+4132	4C 41.21		Y		FR II	Q	22	22
1015+359	J1018+3542	B2 1015+35B		Y		CT,CFS	Q		41,42
1020+400	J1023+3948	4C +40.25		Y		CT,CFS	Q		41,42
1030+415	J1033+4116	IVS B1030+415		Y		CT ,CSF	Q		41,42
1030+585	J1033+5814	3C 244.1		Y	Y	FR II	G	8,9	
1031+567	J1035+5628	JVAS J1035+5628	Y		Y	CSO	G ^a		65, 67
1040+12	J1042+1203	3C 245			Y [†]	D	Q	8,9	
1039+811	J1044+8054	S5 1039+81		Y		CT,CFS	Q		42
1044+719	J1048+7143	S5 1044+71		Y		CT,CFS	Q		41,42
1053+704	J1056+7011	S5 1053+70		Y		CT,CFS	Q		41,42
1053+815	J1058+8114	S5 1053+81		Y		CT,CFS	G		41,42
1055+20	J1058+1951	4C 20.24			Y	D	Q	9	58
1056+432	J1058+4301	3C 247		Y	Y	FR II	G	9,40,62	
1058+726	J1101+7225	S5 1058+726		Y		CT,CSS	Q		41,42
1100+772	J1104+7658	3C 249.1		Y		FR II	Q	37	
1101+384	J1104+3812	Mrk 421		Y		CT,CFS	Q		41,42
1111+408	J1114+4037	3C 254		Y		FR II	Q	55	
1116+12	J1118+1234	4C 12.39			Y [†]	U,CFS	Q	9	21
1128+385	J1130+3815	IVS B1128+385		Y		CT,CFS	Q		41,42
1137+660	J1139+6547	3C 263		Y	Y	FR II	Q	9,37	
1138+594	J1140+5912	4C +59.16		Y		CT,CSS			41,42
1140+22	J1143+2206	3C 263.1			Y	FR II	G	8,9	
1142+19	J1145+1936	3C 264			Y [†]	FR I	G	9,26	
1144+542	J1146+5356	S4 1144+54		Y		CT,CSS	Q		41,42
1144+402	J1146+3958	S4 1144+40		Y		CT,CFS	Q		41,42
1150+812	J1153+8058	S5 1150+81		Y		CT,CFS	Q		58
1150+497	J1153+4931	4C 49.22		Y	Y	CSS	Q	9	41,42
1152+551	J1155+5453	4C +55.22		Y		Complex	G	16	
1153+31	J1156+3128	4C 31.38			Y	CSS	Q	9,57	
1157+732	J1200+7300	3C 268.1	Y		Y	FR II	G ^a	8,9,62	
1203+645	J1206+6413	3C 268.3		Y	Y	CSS	G	9,48	
1213+538	J1215+5335	4C +53.24		Y		FR II	Q	44	

Table 7 continued

Table 7 (continued)

B1950 Name	J2000 Name	Alias	PR	CJ1	PW	Type	Optical ID [†]	Large-scale Structure	Small-scale Structure
(1)	(2)	(3)	(4)	(5)	(6)	(7)	(8)	(9)	(10)
1213+350	J1215+3448	S4 1213+350		Y		CT,CFS	Q		41,42
1216+487	J1219+4829	S4 1216+48		Y		CT,CFS	Q		41,42
1218+33	J1220+3343	3C 270.1			Y	FR II	Q	8,9,62	
1222+13	J1225+1253	3C 272.1			Y [†]	FR I	G	8,9	
1225+368	J1227+3635	B2 1225+36		Y	Y	CSO	Q ^b		54, 56, 70
1228+12	J1230+1223	3C 274			Y [†]	FR I	G	1,9	
1241+16	J1243+1622	3C 275.1			Y	FR II	Q	8,9,62	
1242+410	J1244+4048	B3 1242+410		Y		CSO	Q		41,42
1250+568	J1252+5634	3C 277.1		Y	Y	CSS	Q	9,43	
1251+27	J1254+2737	3C 277.3			Y	FR II	G	3,9	
1254+476	J1256+4720	3C 280	Y		Y	FR II	G	9,17	
1311+678	J1313+6736	4C +67.22		Y		CSS		9	41,42
1317+520	J1319+5148	4C +52.27		Y		CT,CFS	Q		41,42
1319+428	J1321+4235	3C 285		Y		FR II	G	50	
1323+32	J1326+3154	DA 344			Y [†]	CSO	G ^a		58, 56, 70
1328+25	J1330+2509	3C 287			Y [†]	CSS	Q	9	58
1328+30	J1331+3030	3C 286			Y [†]	CSS	Q	9,48	
1333+459	J1335+4542	S4 1333+459		Y		CT,CFS	Q		41,42
1333+589	J1335+5844	JVAS J1335+5844		Y		CSO			41,42
1336+391	J1338+3851	3C 288		Y	Y	FR ?	G	9,32	
1342+663	J1344+6606	S4 1342+663		Y		CT,CFS	Q		41,42
1345+12	J1347+1217	PKS B1345+125			Y [†]	CSO	G	71	58
1347+539	J1349+5341	4C 53.28		Y		CT,CFS	Q		41,42,72
1349+647	J1350+6429	3C 292		Y		FR II	G	30	
1350+31	J1352+3126	3C 293			Y [†]	FR ?	G	9,43	
1354+19	J1357+1919	4C 19.44			Y [†]	FR II	Q	9	58
1357+769	J1357+7643	S5 1357+76		Y		CT,CFS	Q		41,42
1358+624	J1400+6210	4C 62.22	Y		Y	CSO	G		56,70
1404+28	J1407+2827	OQ 208			Y [†]	CSO	G		58, 72
1409+524	J1411+5212	3C 295	Y		Y	FR II	G	9,17	
1413+34	J1416+3444	B2 1413+34			Y	CSO	EF ^a		54,56
1414+11	J1416+1048	3C 296			Y [†]	FR I	G	9,34	
1418+546	J1419+5423	OQ 530		Y		CT,CFS	Q		41,42
1419+419	J1421+4144	3C 299		Y	Y	CSS	G	9,43	
1420+19	J1422+1935	3C 300			Y	FR II	G	9,29,64	
1435+638	J1436+6336	VIPS 0792		Y		CT,CFS	Q		41,42
1437+624	J1438+6211	OQ 663		Y		CT,CSS	Q		41,42
1438+385	J1440+3820	S4 1438+38		Y		CT,CFS	Q		41,42
1441+522	J1443+5201	3C 303		Y	Y	FR II	G	9,17	

Table 7 continued

Table 7 (*continued*)

B1950 Name	J2000 Name	Alias	PR	CJ1	PW	Type	Optical ID [†]	Large-scale Structure	Small-scale Structure
(1)	(2)	(3)	(4)	(5)	(6)	(7)	(8)	(9)	(10)
1442+10	J1445+0958	OQ 172			Y	CSS	Q	9	51,56
1448+634	J1449+6316	3C 305		Y	Y	FR ?	G	9,17	
1458+718	J1459+7140	3C 309.1	Y		Y	CSS	Q	9,48	31
1502+10	J1504+1029	4C 10.39			Y [†]	U,CFS	Q	9	58
1502+26	J1504+2600	3C 310			Y [†]	FR II	G	27	
1504+377	J1506+3730	B2 1504+37		Y		CT,CFS	G		41,42
1511+26	J1513+2607	3C 315			Y	FR ?	G	9,29	
1529+24	J1531+2404	3C 321			Y	FR II	G	8,9	
1538+14	J1540+1447	4C 14.60			Y [†]	U,CFS	Q?	9	58
1547+507	J1549+5038	S4 1547+507		Y		CT,CFS	Q		41,42
1549+628	J1549+6241	3C 325		Y	Y	FR II	G	8,9	
1557+708	J1557+7041	NGC 6048		Y	Y	FR I	G	9,19	
1600+33	J1602+3326	4C +33.38			Y [†]	CSS	G ^a	9	54,56
1607+26	J1609+2641	CTD 93			Y [†]	CSO	G ^a		58,73
1609+660	J1609+6556	3C 330	Y		Y	FR II	G	8	
1611+34	J1613+3412	DA 406			Y [†]	CT,CFS	Q		58
1624+416	J1625+4134	4C 41.32	Y		Y	U,CFS	Q ^a	9	31
1627+444	J1628+4419	3C 337		Y	Y	FR II	G	8,9	
1637+826	J1632+8232	NGC 6251		Y	Y	FR ?	G	11	
1634+628	J1634+6245	3C 343	Y		Y	CSS	Q	9,57	
1633+382	J1635+3808	4C 38.41	Y		Y	U,CFS	Q		31
1637+574	J1638+5720	OS 562	Y			CT,CFS	Q		31
1637+626	J1638+6234	3C 343.1		Y	Y	CSS	G	9,57	
1638+398	J1640+3946	NRAO 512		Y		CT,CFS	Q		41,42
1642+690	J1642+6856	4C 69.21	Y			CT,CFS	Q		31
1641+399	J1642+3948	3C 345	Y		Y	U,CFS	Q	9	58
1641+17	J1643+1715	3C 346			Y [†]	FR I	G	3,9	
1652+398	J1653+3945	Mrk 501	Y			CT,CFS	G		31
1656+482	J1657+4808	4C +48.41		Y		CT,CFS			41,42
1656+477	J1658+4737	S4 1656+47		Y		CT,CFS	Q		41,42
1658+471	J1659+4702	3C 349		Y	Y	FR II	G	8,9,64	
1704+608	J1704+6044	3C 351		Y	Y	FR II	Q	4,9	
1719+357	J1721+3542	S4 1719+357		Y		CT,CFS	Q		41,42
1726+31	J1728+3145	3C 357			Y	FR II	G	1,9	
1732+389	J1734+3857	OT 355		Y		CT,CFS	Q		41,42
1734+508	J1735+5049			Y		CSO			41,42,74
1738+476	J1739+4737	OT 465		Y		CT,CFS	Q		41,42
1739+522	J1740+5211	4C 51.37	Y		Y	U,CFS	Q	9	31
1749+701	J1748+7005	S4 1749+70	Y		Y	CSS	Q	9	31

Table 7 (*continued*)

Table 7 (continued)

B1950 Name	J2000 Name	Alias	PR	CJ1	PW	Type	Optical ID [‡]	Large-scale Structure	Small-scale Structure
(1)	(2)	(3)	(4)	(5)	(6)	(7)	(8)	(9)	(10)
1751+441	J1753+4409	S4 1751+441		Y		CT,CFS	Q		41,42
1758+388	J1800+3848	B3 1758+388B		Y		CT,CFS	Q		41,42
1803+784	J1800+7828	S5 1803+784	Y		Y	U,CFS	Q	9	31
1800+440	J1801+4404	S4 1800+44		Y		CT,CFS	Q		41,42
1807+698	J1806+6949	3C 371	Y		Y	U,CFS	G	9	31
1819+396	J1821+3942	4C 39.56		Y	Y	CSS	G?	9,57,56	
1823+568	J1824+5651	4C 56.27	Y		Y	U,CFS	Q	9	31
1825+743	J1824+7420	3C 379.1		Y		FR II	G	1	
1828+487	J1829+4844	3C 380	Y		Y	D	Q	9,48	
1829+29	J1831+2907	4C 29.56			Y	CSS	G ^a	9,57,56	
1833+653	J1833+6521	3C 383		Y		FR II	G	12	
1832+474	J1833+4727	3C 381		Y	Y	FR II	G	9,17,64	
1845+797	J1842+7946	3C 390.3	Y		Y	FR II	G	9,17	31
1842+681	J1842+6809	TXS 1842+681		Y		CT,CFS	Q		41,42
1842+455	J1844+4533	3C 388	Y		Y	FR II	G	9,17	
1843+356	J1845+3541	COINS J1845+3541		Y		CT,CFS	G		41,42
1926+611	J1927+6117	S4 1926+61		Y		CT,CFS	Q		41,42
1928+738	J1927+7358	4C 73.18	Y		Y	U,CFS	Q	9	31
1939+605	J1940+6041	3C 401	Y		Y	FR II	G	8,9,64	
1940+504	J1941+5035	3C 402		Y		FR ?	G	4	
1943+546	J1944+5448	COINS J1944+5448		Y		CSO	G		41,42
1954+513	J1955+5131	OV 591	Y		Y	U,CFS	Q	9	31
2007+777	J2005+7752	S5 2007+77		Y		CT,CFS	Q		58
2010+723	J2009+7229	4C +72.28		Y		CT,CFS	Q		41,42
2021+614	J2022+6136	TXS 2021+614	Y		Y	CSO	G		31,41
2104+763	J2104+7633	3C 427.1		Y	Y	FR II	G	9,17	
2121+24	J2123+2504	3C 433			Y [†]	FR ?	G	3,9	
2141+27	J2144+2810	3C 436			Y	FR II	G	4,9,64	
2145+15	J2147+1520	3C 437			Y	FR II	G	5,9	
2153+377	J2155+3800	3C 438	Y		Y	FR II	G	9,17,64	
2200+420	J2202+4216	BL Lac	Y		Y	U,CFS	Q	9	58
2203+29	J2206+2929	3C 441			Y	FR II	G	5,9	
2207+374	J2209+3742	S4 2207+37		Y		CT,CSS	Q		41,42
2214+350	J2216+3518	OY 324		Y		CT,CFS	Q		41,42
2229+695	J2230+6946	S5 2229+69		Y		CT,CFS	G		41,42
2229+391	J2231+3921	3C 449	Y		Y	FR I	G	9,18	
2230+11	J2232+1143	CTA 102			Y [†]	U,CFS	Q	9	58,56
2243+394	J2245+3941	3C 452	Y		Y	FR II	G	1,9	
2247+14	J2250+1419	4C 14.82			Y	CSS	Q	9	38

Table 7 continued

Table 7 (*continued*)

B1950 Name	J2000 Name	Alias	PR	CJ1	PW	Type	Optical ID [‡]	Large-scale Structure	Small-scale Structure
(1)	(2)	(3)	(4)	(5)	(6)	(7)	(8)	(9)	(10)
2251+15	J2253+1608	3C 454.3			Y [†]	U,CFS	Q	9,58	
2252+12	J2255+1313	3C 455			Y	FR II	Q	9	63
2253+417	J2255+4202	OY 489		Y		CT,CFS	Q		41,42
2255+416	J2257+4154	4C 41.45		Y		CT,CSS	Q		41,42
2311+469	J2313+4712	4C 46.47		Y		CT,CSS	Q		41,42
2323+435	J2325+4346	S4 2323+43		Y		CSS	G	45	
2324+405	J2326+4048	3C 462		Y	Y	FR II	G ^a	9	19
2335+26	J2338+2701	3C 465			Y [†]	FR I	G	1,9	
2342+821	J2344+8226	S5 2342+82	Y		Y	CSS	Q ^a	9,57,56	
2351+456	J2354+4553	4C 45.51	Y		Y	U,CFS	Q ^a	9	31
2352+495	J2355+4950	DA 611	Y		Y	CSO	G		31,75

NOTE—* M82 s not an active galaxy, and was therefore not included in the statistical analyses in this paper. [†] indicates objects in the PWS subsample (see text). [‡] the references for the optical classes are as follows: We used the PW (Peacock & Wall 1981) optical identifications where available, otherwise the PR (Pearson & Readhead 1981) and CJ1 (Polatidis et al. 1995), where we replaced “SO” and “BL” entires with “Q”. The only exceptions are ^a from Stickel et al. (1994), and ^b from Peck & Taylor (2000). The columns are as follows: Source Names (1–3), Membership in the PR, CJ1 and PW Samples (4–6), Source Type (7), The Types listed in column (7) are as follows: Quasars (Q), galaxies (G), bona fide CSO (CSO), Fanaroff and Riley types I, II and intermediate (FR I, FR II, FR?); objects unresolved by Peacock & Wall (1981) on the 5 km Telescope (U,CSS or U,CFS for compact steep spectrum and compact flat spectrum sources, respectively), doubles indentified by Peacock & Wall (1981) in which the optical ID coincides with one of the radio components (D2); Compact Steep Spectrum objects identified by Peacock & Wall (1981) (CSS); Objects found to be compact in various VLBI surveys other than any identified by Peacock & Wall (1981) (CT,CSS or CT,CFS) for compact steep spectrum and compact flat spectrum sources, respectively; CSO Catalog ID (8), Optical Identifications (9), and Structure References (10+11). No attempt has been made at complete map references for each object since these number in the tens for many objects and the purpose of this Table is solely to provide justification for the claim that the structures of all of these sources are well known. References: 1 MacDonald et al. (1968); 2 Branson et al. (1972); 3 Pooley & Henbest (1974); 4 Riley & Pooley (1975); 5 Longair (1975); 6 Miley et al. (1975); 7 Bridle et al. (1976); 8 Jenkins et al. (1977); 9 Peacock & Wall (1981); 10 Cottrell (1977); 11 Waggett et al. (1977); 12 Fomalont et al. (1980); 13 Burns & Christiansen (1980); 14 Pearson & Readhead (1981); 15 Porcas (1981); 16 Kapahi (1981); 17 Laing (1981); 18 Birkinshaw et al. (1981); 19 Peacock & Wall (1982); 20 Laing et al. (1983); 21 Romney et al. (1984); 22 Owen & Puschell (1984); 23 Spangler et al. (1984); 24 Strom & Willis (1980); 25 Lonsdale (1984); 26 Jenkins (1982); 27 van Breugel & Fomalont (1984); 28 Fanti et al. (1986); 29 Leahy et al. (1986); 30 Alexander & Leahy (1987); 31 Pearson & Readhead (1988); 32 Bridle et al. (1989); 33 Pedlar et al. (1990); 34 Leahy & Perley (1991); 35 Altschuler et al. (1995a); 36 Turland (1975); 37 Bridle et al. (1994); 38 Lister et al. (1994); 39 Giovannini et al. (1994); 40 Akujor et al. (1994); 41 Polatidis et al. (1995) or (Thakkar et al. 1995); 42 Xu et al. (1995); 43 Akujor & Garrington (1995); 44 Reid et al. (1995); 45 Sanghera et al. (1995); 46 Hardcastle et al. (1996); 47 Leahy et al. (1997); 48 Ludke et al. (1998); 49 Neff et al. (1995); 50 Dennett-Thorpe et al. (1999); 51 Fomalont et al. (2000); 52 Looney & Hardcastle (2000); 53 Saikia et al. (2001); 54 Dallacasa et al. (2013); 55 Thomasson et al. (2006); 56 Dallacasa et al. (1995); 57 Dallacasa et al. (2021); 58 MOJAVE website: <https://www.cv.nrao.edu/MOJAVE/allsources.html>; 59 Radio Fundamental Catalog (RFC); 60 Kellermann et al. (1998); 61 Giovannini et al. (2018); 62 Fernini (2014); 63 Akujor et al. (1991); 64 (Hardcastle et al. 1997); 65 Tremblay et al. (2016); 66 Baum et al. (1990); 67 Sokolovsky et al. (2011); 68 Altschuler et al. (1995b); 69 Xu (1995); 70 Dallacasa et al. (1995); 71 Stanghellini et al. (2005); 72 Xiang et al. (2002); 73 Nagai et al. (2006); 74 Orienti & Dallacasa (2014); 75 Readhead et al. (1996)

REFERENCES

- Akujor, C. E., & Garrington, S. T. 1995, *A&AS*, 112, 235
- Akujor, C. E., Luedke, E., Browne, I. W. A., et al. 1994, *A&AS*, 105, 247
- Akujor, C. E., Spencer, R. E., Zhang, F. J., et al. 1991, *MNRAS*, 250, 215, doi: [10.1093/mnras/250.1.215](https://doi.org/10.1093/mnras/250.1.215)
- Alexander, P., & Leahy, J. P. 1987, *MNRAS*, 225, 1, doi: [10.1093/mnras/225.1.1](https://doi.org/10.1093/mnras/225.1.1)
- Altschuler, D. R., Gurvits, L. I., Alef, W., et al. 1995a, *A&AS*, 114, 197
- . 1995b, *A&AS*, 114, 197
- An, T., & Baan, W. A. 2012, *ApJ*, 760, 77, doi: [10.1088/0004-637X/760/1/77](https://doi.org/10.1088/0004-637X/760/1/77)
- Augusto, P. 2009, *Astronomische Nachrichten*, 330, 190, doi: [10.1002/asna.200811153](https://doi.org/10.1002/asna.200811153)
- Augusto, P., Gonzalez-Serrano, J. I., Perez-Fournon, I., & Wilkinson, P. N. 2006, *MNRAS*, 368, 1411, doi: [10.1111/j.1365-2966.2006.10227.x](https://doi.org/10.1111/j.1365-2966.2006.10227.x)
- Augusto, P., Wilkinson, P. N., & Browne, I. W. A. 1998, *MNRAS*, 299, 1159, doi: [10.1046/j.1365-8711.1998.01871.x](https://doi.org/10.1046/j.1365-8711.1998.01871.x)
- Baum, S. A., O’Dea, C. P., Murphy, D. W., & de Bruyn, A. G. 1990, *A&A*, 232, 19
- Birkinshaw, M., Laing, R. A., & Peacock, J. A. 1981, *MNRAS*, 197, 253, doi: [10.1093/mnras/197.2.253](https://doi.org/10.1093/mnras/197.2.253)
- Blandford, R., Meier, D., & Readhead, A. 2019, *ARA&A*, 57, 467, doi: [10.1146/annurev-astro-081817-051948](https://doi.org/10.1146/annurev-astro-081817-051948)
- Branson, N. J. B. A., Elsmore, B., Pooley, G. G., & Ryle, M. 1972, *MNRAS*, 156, 377, doi: [10.1093/mnras/156.4.377](https://doi.org/10.1093/mnras/156.4.377)
- Bridle, A. H., Davis, M. M., Meloy, D. A., et al. 1976, *Nature*, 262, 179, doi: [10.1038/262179a0](https://doi.org/10.1038/262179a0)
- Bridle, A. H., Fomalont, E. B., Byrd, G. G., & Valtonen, M. J. 1989, *AJ*, 97, 674, doi: [10.1086/115013](https://doi.org/10.1086/115013)
- Bridle, A. H., Hough, D. H., Lonsdale, C. J., Burns, J. O., & Laing, R. A. 1994, *AJ*, 108, 766, doi: [10.1086/117112](https://doi.org/10.1086/117112)
- Burns, J. O., & Christiansen, W. A. 1980, *Nature*, 287, 208, doi: [10.1038/287208a0](https://doi.org/10.1038/287208a0)
- Callingham, J. R., Ekers, R. D., Gaensler, B. M., et al. 2017, *ApJ*, 836, 174, doi: [10.3847/1538-4357/836/2/174](https://doi.org/10.3847/1538-4357/836/2/174)
- Carilli, C. L., Perley, R. A., Dreher, J. W., & Leahy, J. P. 1991, *ApJ*, 383, 554, doi: [10.1086/170813](https://doi.org/10.1086/170813)
- Cohen, A. M., Porcas, R. W., Browne, I. W. A., Daintree, E. J., & Walsh, D. 1977, *MmRAS*, 84, 1
- Cottrell, G. A. 1977, *MNRAS*, 178, 577, doi: [10.1093/mnras/178.4.577](https://doi.org/10.1093/mnras/178.4.577)
- Curtis, H. D. 1918, *Publications of Lick Observatory*, 13, 9
- Dallacasa, D., Fanti, C., Fanti, R., Schilizzi, R. T., & Spencer, R. E. 1995, *A&A*, 295, 27
- Dallacasa, D., Orienti, M., Fanti, C., & Fanti, R. 2021, *MNRAS*, 504, 2312, doi: [10.1093/mnras/stab1014](https://doi.org/10.1093/mnras/stab1014)
- Dallacasa, D., Orienti, M., Fanti, C., Fanti, R., & Stanghellini, C. 2013, *MNRAS*, 433, 147, doi: [10.1093/mnras/stt710](https://doi.org/10.1093/mnras/stt710)
- Dennett-Thorpe, J., Bridle, A. H., Laing, R. A., & Scheuer, P. A. G. 1999, *MNRAS*, 304, 271, doi: [10.1046/j.1365-8711.1999.02234.x](https://doi.org/10.1046/j.1365-8711.1999.02234.x)
- Dent, W. A. 1965a, *Science*, 148, 1458, doi: [10.1126/science.148.3676.1458](https://doi.org/10.1126/science.148.3676.1458)
- . 1965b, *AJ*, 70, 672, doi: [10.1086/109792](https://doi.org/10.1086/109792)
- Fanaroff, B. L., & Riley, J. M. 1974, *MNRAS*, 167, 31P, doi: [10.1093/mnras/167.1.31P](https://doi.org/10.1093/mnras/167.1.31P)
- Fanti, C., Fanti, R., Dallacasa, D., et al. 1995, *A&A*, 302, 317
- Fanti, C., Fanti, R., de Ruiter, H. R., & Parma, P. 1986, *A&AS*, 65, 145
- Fanti, C., Fanti, R., Parma, P., Schilizzi, R. T., & van Breugel, W. J. M. 1985, *A&A*, 143, 292
- Fanti, R., Fanti, C., Schilizzi, R. T., et al. 1990, *A&A*, 231, 333
- Fernini, I. 2014, *ApJS*, 212, 19, doi: [10.1088/0067-0049/212/2/19](https://doi.org/10.1088/0067-0049/212/2/19)
- Fomalont, E. B., Frey, S., Paragi, Z., et al. 2000, *ApJS*, 131, 95, doi: [10.1086/317368](https://doi.org/10.1086/317368)
- Fomalont, E. B., Palimaka, J. J., & Bridle, A. H. 1980, *AJ*, 85, 981, doi: [10.1086/112761](https://doi.org/10.1086/112761)
- Förster Schreiber, N. M., & Wuyts, S. 2020, *ARA&A*, 58, 661, doi: [10.1146/annurev-astro-032620-021910](https://doi.org/10.1146/annurev-astro-032620-021910)
- Giovannini, G., Feretti, L., Venturi, T., et al. 1994, *ApJ*, 435, 116, doi: [10.1086/174799](https://doi.org/10.1086/174799)
- Giovannini, G., Savolainen, T., Orienti, M., et al. 2018, *Nature Astronomy*, 2, 472, doi: [10.1038/s41550-018-0431-2](https://doi.org/10.1038/s41550-018-0431-2)
- Gregory, P. C., Scott, W. K., Douglas, K., & Condon, J. J. 1996, *ApJS*, 103, 427, doi: [10.1086/192282](https://doi.org/10.1086/192282)
- Hardcastle, M. J., Alexander, P., Pooley, G. G., & Riley, J. M. 1996, *MNRAS*, 278, 273, doi: [10.1093/mnras/278.1.273](https://doi.org/10.1093/mnras/278.1.273)
- . 1997, *MNRAS*, 288, 859, doi: [10.1093/mnras/288.4.859](https://doi.org/10.1093/mnras/288.4.859)
- Helmboldt, J. F., Taylor, G. B., Tremblay, S., et al. 2007, *ApJ*, 658, 203, doi: [10.1086/511005](https://doi.org/10.1086/511005)
- Hubble, E. 1929a, *Proceedings of the National Academy of Science*, 15, 168, doi: [10.1073/pnas.15.3.168](https://doi.org/10.1073/pnas.15.3.168)
- . 1929b, *Contributions from the Mount Wilson Observatory*, 3, 23
- Jenkins, C. J., Pooley, G. G., & Riley, J. M. 1977, *MmRAS*, 84, 61

- Jenkins, C. R. 1982, *MNRAS*, 200, 705, doi: [10.1093/mnras/200.3.705](https://doi.org/10.1093/mnras/200.3.705)
- Kapahi, V. K. 1981, *A&AS*, 43, 381
- Kellermann, K. I., & Pauliny-Toth, I. I. K. 1969, *ApJL*, 155, L71, doi: [10.1086/180305](https://doi.org/10.1086/180305)
- Kellermann, K. I., Vermeulen, R. C., Zensus, J. A., & Cohen, M. H. 1998, *AJ*, 115, 1295, doi: [10.1086/300308](https://doi.org/10.1086/300308)
- Komatsu, E., Dunkley, J., Nolta, M. R., et al. 2009, *ApJS*, 180, 330, doi: [10.1088/0067-0049/180/2/330](https://doi.org/10.1088/0067-0049/180/2/330)
- Kuehr, H., Pauliny-Toth, I. I. K., Witzel, A., & Schmidt, J. 1981, *AJ*, 86, 854, doi: [10.1086/112957](https://doi.org/10.1086/112957)
- Laing, R. A. 1981, *MNRAS*, 195, 261, doi: [10.1093/mnras/195.2.261](https://doi.org/10.1093/mnras/195.2.261)
- Laing, R. A., Riley, J. M., & Longair, M. S. 1983, *MNRAS*, 204, 151, doi: [10.1093/mnras/204.1.151](https://doi.org/10.1093/mnras/204.1.151)
- Lawrence, C. R., Zucker, J. R., Readhead, A. C. S., et al. 1996, *ApJS*, 107, 541, doi: [10.1086/192375](https://doi.org/10.1086/192375)
- Leahy, J. P., Black, A. R. S., Dennett-Thorpe, J., et al. 1997, *MNRAS*, 291, 20, doi: [10.1093/mnras/291.1.20](https://doi.org/10.1093/mnras/291.1.20)
- Leahy, J. P., & Perley, R. A. 1991, *AJ*, 102, 537, doi: [10.1086/115892](https://doi.org/10.1086/115892)
- Leahy, J. P., Pooley, G. G., & Riley, J. M. 1986, *MNRAS*, 222, 753, doi: [10.1093/mnras/222.4.753](https://doi.org/10.1093/mnras/222.4.753)
- Lister, M. L., Aller, M. F., Aller, H. D., et al. 2018, *ApJS*, 234, 12, doi: [10.3847/1538-4365/aa9c44](https://doi.org/10.3847/1538-4365/aa9c44)
- Lister, M. L., Gower, A. C., & Hutchings, J. B. 1994, *AJ*, 108, 821, doi: [10.1086/117113](https://doi.org/10.1086/117113)
- Lister, M. L., Homan, D. C., Hovatta, T., et al. 2019, *ApJ*, 874, 43, doi: [10.3847/1538-4357/ab08ee](https://doi.org/10.3847/1538-4357/ab08ee)
- Longair, M. S. 1975, *MNRAS*, 173, 309, doi: [10.1093/mnras/173.2.309](https://doi.org/10.1093/mnras/173.2.309)
- Longair, M. S., & Scheuer, P. A. G. 1970, *MNRAS*, 151, 45, doi: [10.1093/mnras/151.1.45](https://doi.org/10.1093/mnras/151.1.45)
- Lonsdale, C. J. 1984, *MNRAS*, 208, 545, doi: [10.1093/mnras/208.3.545](https://doi.org/10.1093/mnras/208.3.545)
- Looney, L. W., & Hardcastle, M. J. 2000, *ApJ*, 534, 172, doi: [10.1086/308753](https://doi.org/10.1086/308753)
- Ludke, E., Garrington, S. T., Spencer, R. E., et al. 1998, *MNRAS*, 299, 467, doi: [10.1046/j.1365-8711.1998.01843.x](https://doi.org/10.1046/j.1365-8711.1998.01843.x)
- MacDonald, G. H., Kenderdine, S., & Neville, A. C. 1968, *MNRAS*, 138, 259, doi: [10.1093/mnras/138.3.259](https://doi.org/10.1093/mnras/138.3.259)
- Miley, G. K., Wellington, K. J., & van der Laan, H. 1975, *A&A*, 38, 381
- Minkowski, R. 1941, *PASP*, 53, 224, doi: [10.1086/125315](https://doi.org/10.1086/125315)
- Nagai, H., Inoue, M., Asada, K., Kamenoi, S., & Doi, A. 2006, *ApJ*, 648, 148, doi: [10.1086/505793](https://doi.org/10.1086/505793)
- Neff, S. G., Roberts, L., & Hutchings, J. B. 1995, *ApJS*, 99, 349, doi: [10.1086/192190](https://doi.org/10.1086/192190)
- Nilsson, K., Valtonen, M. J., Kotilainen, J., & Jaakkola, T. 1993, *ApJ*, 413, 453, doi: [10.1086/173016](https://doi.org/10.1086/173016)
- O’Dea, C. P., & Saikia, D. J. 2021a, *A&A Rv*, 29, 3, doi: [10.1007/s00159-021-00131-w](https://doi.org/10.1007/s00159-021-00131-w)
- . 2021b, *A&A Rv*, 29, 3, doi: [10.1007/s00159-021-00131-w](https://doi.org/10.1007/s00159-021-00131-w)
- Orienti, M., & Dallacasa, D. 2014, *MNRAS*, 438, 463, doi: [10.1093/mnras/stt2217](https://doi.org/10.1093/mnras/stt2217)
- Owen, F. N., & Puschell, J. J. 1984, *AJ*, 89, 932, doi: [10.1086/113589](https://doi.org/10.1086/113589)
- Owsianik, I., & Conway, J. E. 1998, *A&A*, 337, 69, <https://arxiv.org/abs/astro-ph/9712062>
- Owsianik, I., Conway, J. E., & Polatidis, A. G. 1999, *NewAR*, 43, 669, doi: [10.1016/S1387-6473\(99\)00075-5](https://doi.org/10.1016/S1387-6473(99)00075-5)
- Pauliny-Toth, I. I. K. 1977, in *Radio Astronomy and Cosmology*, ed. D. L. Jauncey, Vol. 74, 63
- Pauliny-Toth, I. I. K., Witzel, A., Preuss, E., et al. 1978, *AJ*, 83, 451, doi: [10.1086/112223](https://doi.org/10.1086/112223)
- Peacock, J. A., & Gull, S. F. 1981, *MNRAS*, 196, 611, doi: [10.1093/mnras/196.3.611](https://doi.org/10.1093/mnras/196.3.611)
- Peacock, J. A., & Wall, J. V. 1981, *MNRAS*, 194, 331, doi: [10.1093/mnras/194.2.331](https://doi.org/10.1093/mnras/194.2.331)
- . 1982, *MNRAS*, 198, 843, doi: [10.1093/mnras/198.3.843](https://doi.org/10.1093/mnras/198.3.843)
- Pearson, T. J., & Readhead, A. C. S. 1981, *ApJ*, 248, 61, doi: [10.1086/159130](https://doi.org/10.1086/159130)
- . 1988, *ApJ*, 328, 114, doi: [10.1086/166274](https://doi.org/10.1086/166274)
- Peck, A. B., & Taylor, G. B. 2000, *ApJ*, 534, 90, doi: [10.1086/308746](https://doi.org/10.1086/308746)
- Pedlar, A., Ghataure, H. S., Davies, R. D., et al. 1990, *MNRAS*, 246, 477
- Planck Collaboration, Aghanim, N., Akrami, Y., et al. 2020, *A&A*, 641, A6, doi: [10.1051/0004-6361/201833910](https://doi.org/10.1051/0004-6361/201833910)
- Polatidis, A. G., Conway, J. E., & Owsianik, I. 2002, in *Proceedings of the 6th EVN Symposium*, 139
- Polatidis, A. G., Wilkinson, P. N., Xu, W., et al. 1995, *ApJS*, 98, 1, doi: [10.1086/192152](https://doi.org/10.1086/192152)
- Pooley, G. G., & Henbest, S. N. 1974, *MNRAS*, 169, 477, doi: [10.1093/mnras/169.3.477](https://doi.org/10.1093/mnras/169.3.477)
- Pooley, G. G., & Ryle, M. 1968, *MNRAS*, 139, 515, doi: [10.1093/mnras/139.4.515](https://doi.org/10.1093/mnras/139.4.515)
- Porcas, R. W. 1981, *Nature*, 294, 47, doi: [10.1038/294047a0](https://doi.org/10.1038/294047a0)
- Press, W. H., Flannery, B. P., Teukolsky, S. A., & Vetterling, W. T. 1992, *Numerical Recipes in FORTRAN 77: The Art of Scientific Computing*, 2nd edn. (Cambridge University Press). <http://www.worldcat.org/isbn/052143064X>
- Rawlings, S., & Saunders, R. 1991, *Nature*, 349, 138, doi: [10.1038/349138a0](https://doi.org/10.1038/349138a0)
- Readhead, A. C. S. 1980, in *Objects of High Redshift*, ed. G. O. Abell & P. J. E. Peebles, Vol. 92, 165–175
- Readhead, A. C. S. 1994, *ApJ*, 426, 51, doi: [10.1086/174038](https://doi.org/10.1086/174038)

- Readhead, A. C. S., Cohen, M. H., Pearson, T. J., & Wilkinson, P. N. 1978, *Nature*, 276, 768, doi: [10.1038/276768a0](https://doi.org/10.1038/276768a0)
- Readhead, A. C. S., Taylor, G. B., Xu, W., et al. 1996, *ApJ*, 460, 612, doi: [10.1086/176996](https://doi.org/10.1086/176996)
- Readhead, A. C. S., Xu, W., Pearson, T. J., Wilkinson, P. N., & Polatidis, A. G. 1994, in *Compact Extragalactic Radio Sources*, ed. J. A. Zensus & K. I. Kellermann, 17
- Readhead, A. C. S., Kiehlmann, S., Lister, M. L., et al. 2021, *Astronomische Nachrichten*, 342, 1185, doi: [10.1002/asna.20210049](https://doi.org/10.1002/asna.20210049)
- Rees, M. J. 1966, *Nature*, 211, 468, doi: [10.1038/211468a0](https://doi.org/10.1038/211468a0)
- . 1967, *MNRAS*, 135, 345, doi: [10.1093/mnras/135.4.345](https://doi.org/10.1093/mnras/135.4.345)
- Reid, A., Shone, D. L., Akujor, C. E., et al. 1995, *A&AS*, 110, 213
- Riley, J. M., & Pooley, G. G. 1975, *MmRAS*, 80, 105
- Romney, J., Padrielli, L., Bartel, N., et al. 1984, *A&A*, 135, 289
- Saikia, D. J., Jeyakumar, S., Salter, C. J., et al. 2001, *MNRAS*, 321, 37, doi: [10.1046/j.1365-8711.2001.04017.x](https://doi.org/10.1046/j.1365-8711.2001.04017.x)
- Sanghera, H. S., Saikia, D. J., Luedke, E., et al. 1995, *A&A*, 295, 629
- Scheuer, P. A. G. 1995, *MNRAS*, 277, 331, doi: [10.1093/mnras/277.1.331](https://doi.org/10.1093/mnras/277.1.331)
- Schmidt, M. 1968, *ApJ*, 151, 393, doi: [10.1086/149446](https://doi.org/10.1086/149446)
- Scott, M. A., & Readhead, A. C. S. 1977, *MNRAS*, 180, 539, doi: [10.1093/mnras/180.4.539](https://doi.org/10.1093/mnras/180.4.539)
- Slob, M. M., Callingham, J. R., Röttgering, H. J. A., et al. 2022, *A&A*, 668, A186, doi: [10.1051/0004-6361/202244651](https://doi.org/10.1051/0004-6361/202244651)
- Sokolovsky, K. V., Kovalev, Y. Y., Pushkarev, A. B., Mimica, P., & Perucho, M. 2011, *A&A*, 535, A24, doi: [10.1051/0004-6361/201015772](https://doi.org/10.1051/0004-6361/201015772)
- Spangler, S. R., Myers, S. T., & Pogge, J. J. 1984, *AJ*, 89, 1478, doi: [10.1086/113649](https://doi.org/10.1086/113649)
- Spencer, R. E., Schilizzi, R. T., Fanti, C., et al. 1991, *MNRAS*, 250, 225, doi: [10.1093/mnras/250.1.225](https://doi.org/10.1093/mnras/250.1.225)
- Stanghellini, C., Bondi, M., Dallacasa, D., et al. 1997, *A&A*, 318, 376
- Stanghellini, C., O’Dea, C. P., Dallacasa, D., et al. 2005, *A&A*, 443, 891, doi: [10.1051/0004-6361:20042226](https://doi.org/10.1051/0004-6361:20042226)
- Stickel, M., Meisenheimer, K., & Kuehr, H. 1994, *A&AS*, 105, 211
- Strom, R. G., & Willis, A. G. 1980, *A&A*, 85, 36
- Tacconi, L. J., Genzel, R., & Sternberg, A. 2020, *ARA&A*, 58, 157, doi: [10.1146/annurev-astro-082812-141034](https://doi.org/10.1146/annurev-astro-082812-141034)
- Taylor, G. B., Readhead, A. C. S., & Pearson, T. J. 1996, *ApJ*, 463, 95, doi: [10.1086/177225](https://doi.org/10.1086/177225)
- Thakkar, D. D., Xu, W., Readhead, A. C. S., et al. 1995, *ApJS*, 98, 33, doi: [10.1086/192153](https://doi.org/10.1086/192153)
- Thomasson, P., Saikia, D. J., & Muxlow, T. W. B. 2006, *MNRAS*, 372, 1607, doi: [10.1111/j.1365-2966.2006.10955.x](https://doi.org/10.1111/j.1365-2966.2006.10955.x)
- Tremblay, S. E., Taylor, G. B., Ortiz, A. A., et al. 2016, *MNRAS*, 459, 820, doi: [10.1093/mnras/stw592](https://doi.org/10.1093/mnras/stw592)
- Turland, B. D. 1975, *MNRAS*, 172, 181, doi: [10.1093/mnras/172.1.181](https://doi.org/10.1093/mnras/172.1.181)
- van Breugel, W., & Fomalont, E. B. 1984, *ApJL*, 282, L55, doi: [10.1086/184304](https://doi.org/10.1086/184304)
- Verkhodanov, O. V., Trushkin, S. A., Andernach, H., & Chernenkov, V. N. 2005, *Bulletin of the Special Astrophysics Observatory*, 58, 118. <https://arxiv.org/abs/0705.2959>
- Waggett, P. C., Warner, P. J., & Baldwin, J. E. 1977, *MNRAS*, 181, 465, doi: [10.1093/mnras/181.3.465](https://doi.org/10.1093/mnras/181.3.465)
- Wall, J. V., & Peacock, J. A. 1985, *MNRAS*, 216, 173, doi: [10.1093/mnras/216.2.173](https://doi.org/10.1093/mnras/216.2.173)
- Wilkinson, P. N., Polatidis, A. G., Readhead, A. C. S., Xu, W., & Pearson, T. J. 1994, *ApJL*, 432, L87, doi: [10.1086/187518](https://doi.org/10.1086/187518)
- Wilkinson, P. N., Readhead, A. C. S., Purcell, G. H., & Anderson, B. 1977, *Nature*, 269, 764, doi: [10.1038/269764a0](https://doi.org/10.1038/269764a0)
- Xiang, L., Stanghellini, C., Dallacasa, D., & Haiyan, Z. 2002, *A&A*, 385, 768, doi: [10.1051/0004-6361:20020162](https://doi.org/10.1051/0004-6361:20020162)
- Xu, W. 1995, PhD thesis, California Institute of Technology
- Xu, W., Readhead, A. C. S., Pearson, T. J., Polatidis, A. G., & Wilkinson, P. N. 1995, *ApJS*, 99, 297, doi: [10.1086/192189](https://doi.org/10.1086/192189)